EXPERIMENTAL STUDY OF TIME REVERSAL INVARIANCE
and
ATOMIC FINAL STATE EFFECTS
in
NUCLEAR TRANSITIONS

Thesis by

James L. Gimlett

In Partial Fulfillment of the Requirements

for the Degree of

Doctor of Philosophy

California Institute of Technology

Pasadena, California

1980

(Submitted May 5, 1980)

ACKNOWLEDGMENTS

I wish to thank Professor Felix Boehm for his encouragement, inspiration, and guidance throughout my studies at Caltech.

Let me also express my deep gratitude to Mr. Herb Henrikson, who has been an indispensable source of ideas, advice, and technical innovation.

I am indebted to Dr. Nim Kwan Cheung for introducing me to the field of ultralow-temperature nuclear physics, and for invaluable help, instruction, and pioneering contribution in the present project.

Special thanks are due Dr. Petr Vogel and fellow graduate student Brian Davis for enlightening discussions, and for conveying to me the results of their atomic final state calculations prior to publication. The help of Mr. Ed Redden and students Steve Kellogg and Nai Kwong with the experiment is gratefully acknowledged. The general assistance and help of Mrs. Elsa Garcia are also deeply appreciated.

I would in addition like to thank collaborator Dr. Jerry Lerner of Argonne National Laboratory for preparation of the implanted ^{131}I sources used in the present experiment.

The financial assistance provided by the California Institute of Technology, the Schlumberger Foundation, and the U.S. Energy Research and Development Agency is gratefully acknowledged.

ABSTRACT

Experiments have been performed to test time reversal invariance in nuclei using gamma transitions of oriented ^{191}Ir and ^{131}Xe. The phase angle η associated with the imaginary part of the ratio of reduced matrix elements of the gamma transition was measured through observation of the angular distribution of the linear polarization from oriented nuclei. Interaction of the gamma ray with the atomic electron cloud can cause an additional phase shift ξ which is indistinguishable from the time-reversal phase η. Such an atomic final state effect has been observed for the 129 keV transition in ^{191}Ir. Nuclear orientation was achieved with a large magnetic field (the hyperfine field of Ir in iron) and low temperature (20 to 30 mK obtained with a dilution refrigerator). A Compton polarimeter was used to measure linear polarization of the E2-M1 gamma ray. The matrix-element ratio was found to have an imaginary part corresponding to a phase angle $(\eta+\xi) = (-4.8 \pm 0.2)\times10^{-3}$. This measurement is in agreement with the most recent final state calculations which give $\xi = (-4.3 \pm 0.4)\times10^{-3}$. A limit $|\eta| < 10^{-3}$ is deduced for the time-reversal phase. In another experiment a phase angle $\eta = (-1.2 \pm 1.1)\times10^{-3}$ was measured for the E2-M1 364 keV transition in ^{131}Xe, for which atomic final state effects are small. Both measurements are consistent with time reversal invariance.

TABLE OF CONTENTS

CHAPTER 1

INTRODUCTION

1.1 General Discussion: T Violation in Physics

The symmetries of time reversal, parity, and charge conjugation play a considerable role in modern physics' understanding of the universe. From the now well-established violation of CP in the K meson system[1] it follows from CPT invariance and from a detailed analysis[2] of the K^o decay parameters irrespective of CPT symmetry that time reversal invariance is violated. Aside from this single instance, however, no breakdown of the time-reversal symmetry has ever been observed. Unlike the case of parity, little understanding of T violation exists after fifteen years of theoretical and experimental effort. The investigation of T invariance with increasingly higher accuracy therefore remains of fundamental interest and importance in the solution of this puzzle.

Theories of CP (and T) nonconservation, based on K^o decay parameters, may be divided into four general categories[3]-[5]:

(1) C and T-violating electromagnetic interactions (with expected coupling strength $g_T \simeq 10^{-3} - 10^{-4}$ relative to the strong interaction; predictions for a neutron electric dipole moment d_n range from 10^{-21} to 10^{-23} e cm. These theories are not gauge renormalizable, however).

(2) C and T-violating millistrong (again with $g_T \simeq 10^{-3} - 10^{-4}$, and an expected dipole moment $d_n \simeq 10^{-23}$).

(3) P and T-violating milliweak ($g_T \simeq 10^{-9}$, $d_n \simeq 10^{-23} - 10^{-24}$).

(4) CP (T)-violating superweak ($g_T \simeq 10^{-15}$, $d_n \simeq 10^{-29}$).

Some 12 orders of magnitude in predicted effects are thus encompassed by T-violating theories, and it is up to experimental physics to resolve this rather unsatisfactory situation.

The search for T violation in nuclear physics has basically been directed along three lines of experiments[4]-[6]:

(1) Tests of "detailed balance" in nuclear reactions (P even, T odd),

(2) Measurement of asymmetric spatial correlations (P even, T odd) in nuclear gamma transitions,

(3) Search for electric dipole moments of nucleons (P odd, T odd).

Probably the most precise and easily interpretable limit on T invariance is that provided by the current limit for the neutron dipole moment $d_n < 1.6 \times 10^{-24}$ e cm[7]. From a dimensional argument we might expect for the P and T violating dipole moment

$$d_n \simeq g_T \, g_P \, e\lambda\!\!\!^{-},$$

where g_T and g_P are T and P-nonconserving coupling strengths relative to the strong interaction, with $g_P \simeq GM^2/4\pi \simeq 10^{-6}$, and $\lambda\!\!\!^{-} \simeq 2 \times 10^{-14}$ cm is the neutron Compton wavelength. The current limit for d_n then gives $g_T < 10^{-4}$ and tends to rule out the electromagnetic and millistrong classes of theories. It should be noted, however, that the predictions of these theories are scarcely less crude than the rough dimensional argument given. The situation cannot be completely resolved on the basis of the current limit for d_n.

Limits derived from the T-odd, P-even "detailed balance" and particularly for the γ-correlation classes of experiments are consistent with T being invariant to a few parts in 10^3. Interpretation of these experiments in terms of a T-violating coupling strength is difficult. From dimensional

arguments[8] we can say that in general the couplings g_T are of the same order of magnitude as the measured T-odd variables, although in some cases much smaller limits on g_T might be obtained because of possible enhancement effects[9]-[11]. The limits on T-odd observables provided by this class of measurement are therefore close to the limits proposed by millistrong and electromagnetic theories and further investigation of T invariance in this area of physics is important in resolving the present situation.

1.2 T Invariance in Nuclear Transitions

In low energy nuclear physics, time reversal noninvariance will manifest itself in a mixed γ transition as follows. Let $A(L\pi)$ and $A(L'\pi')$ denote the reduced matrix elements of the two competing multipoles of the transition. The "mixing ratio" δ is defined as

$$\begin{aligned}\delta &= A(L'\pi')/A(L\pi) \\ &= \pm|\delta|e^{i\eta}. \end{aligned} \tag{1.1}$$

A nonvanishing value of the phase η would be evidence for T violation[12].

The imaginary component of δ (i.e. $\sin\eta$) appears in observables which change sign under the T operation; in particular it appears in T-odd correlations involving at least three vectors from the measurable quantities of nuclear spin $\vec{J}$, photon momentum $\vec{k}$, and photon linear or circular polarization $\vec{E}$ or $\vec{S}$. T-odd observables are tabulated in Refs. (13) and (14). Most correlation experiments involve the preparation of a polarized initial state (from which $\vec{J}$ is determined), and the measurement of two other vectors.

One class of experiment involves the search for a T-odd correlation of the form

$$(\langle\vec{J}\rangle \cdot \vec{k}_1 \times \vec{k}_2)(\vec{k}_1 \cdot \vec{k}_2) , \tag{1.2}$$

where $\vec{k}_1$ and $\vec{k}_2$ are the momenta of two cascading gamma rays, measured in coincidence. Polarization of the initial nuclear state ($\langle\vec{J}\rangle$) is obtained by one of three methods: (1) observation of a preceding β decay; (2) capture of polarized neutrons; or (3) cryogenic cooling of the nuclei to low temperature under a strong magnetic field. The low statistical accuracy of such coincident experiments tends to limit the experimental precision, however.

The second major class of experiment involves the measurement of photon polarization $\vec{E}$ in addition to photon momentum $\vec{k}$ in T-odd correlations of the form

$$(\langle\vec{J}\rangle \cdot \vec{k} \times \vec{E})(\langle\vec{J}\rangle\cdot\vec{k})(\langle\vec{J}\rangle\cdot\vec{E}) \ . \qquad (1.3)$$

Mossbauer experiments[15]-[17] which measure the absorption of linearly polarized recoilless γ rays in a magnetic medium are based on this correlation. Because this is a singles counting experiment, fairly high precision may be achieved [e.g. $\sin\eta = (1.0 \pm 1.7) \times 10^{-3}$ for the 90 keV Mossbauer transition in ^{99}Ru[15]]. More recently an experimental technique has been developed for the precise measurement of the correlation (1.3) in the angular distribution of radiation emitted from nuclei polarized by low temperature nuclear orientation[18],[19]. Again a singles counting experiment, this technique yielded for the mixed 122 keV transition in ^{57}Fe the most precise limit to date on an imaginary component of the matrix-element ratio δ with $\sin\eta = (-3.1 \pm 6.5) \times 10^{-4}$.

The work of this thesis is an extension of the above technique to two cases in ^{131}Xe and ^{191}Ir. A limit for $\sin\eta$ is obtained for a mixed transition in ^{131}Xe; for the transition in ^{191}Ir we report[20] the first precise measurement of a nonzero phase for the matrix-element ratio δ, and hence the first observation of a nonvanishing T-odd correlation of the form (1.3). As it turns out, the observed phase can be attributed to atomic final state effects, which are described in the following section.

1.3 Final State Effects That Simulate T Violation

Photons emitted in a nuclear transition may interact with the atomic electrons. As first pointed out by Hannon and Trammell[21] (and Henley and Jacobsohn[22] in reference to nuclear final state effects), virtual scattering processes (indistinguishable final states) of this type will interfere with direct photon emission and give rise to a phase shift ξ between the multipole transition amplitudes of a mixed transition which is indistinguishable from the time-reversal phase η in a correlation experiment.

Photon emission in a nuclear transition is shown schematically in Fig. 1. Diagram (a) represents the amplitude $T_{fi}(L\pi)$ for direct emission of a photon of polarity $(L\pi)$ in the deexcitation of a nucleus in initial state i to final state f. The virtual interaction of the photon with the bound atomic electron is represented in lowest order by diagrams (b) and (c), for which the transition amplitude may be written[23]

$$\Delta T_{fi}(L\pi) = T_{fi}(L\pi)[\rho(L\pi) + i\xi(L\pi)], \tag{1.4}$$

with ρ and $\xi \ll 1$. The imaginary component corresponds to the absorptive part of (b) and (c) from intermediate states on mass shell. The sum of all three diagrams yields for the total transition amplitude

$$\begin{aligned} T'_{fi}(L\pi) &= T_{fi}(L\pi) + \Delta T_{fi}(L\pi) \\ &\simeq T_{fi}(L\pi)e^{i\xi(L\pi)}. \end{aligned} \tag{1.5}$$

With $A(L\pi) \propto T(L\pi)$, the mixing ratio δ of (1.1) becomes

$$\delta = \pm|\delta|e^{i(\eta+\xi)}, \tag{1.6}$$

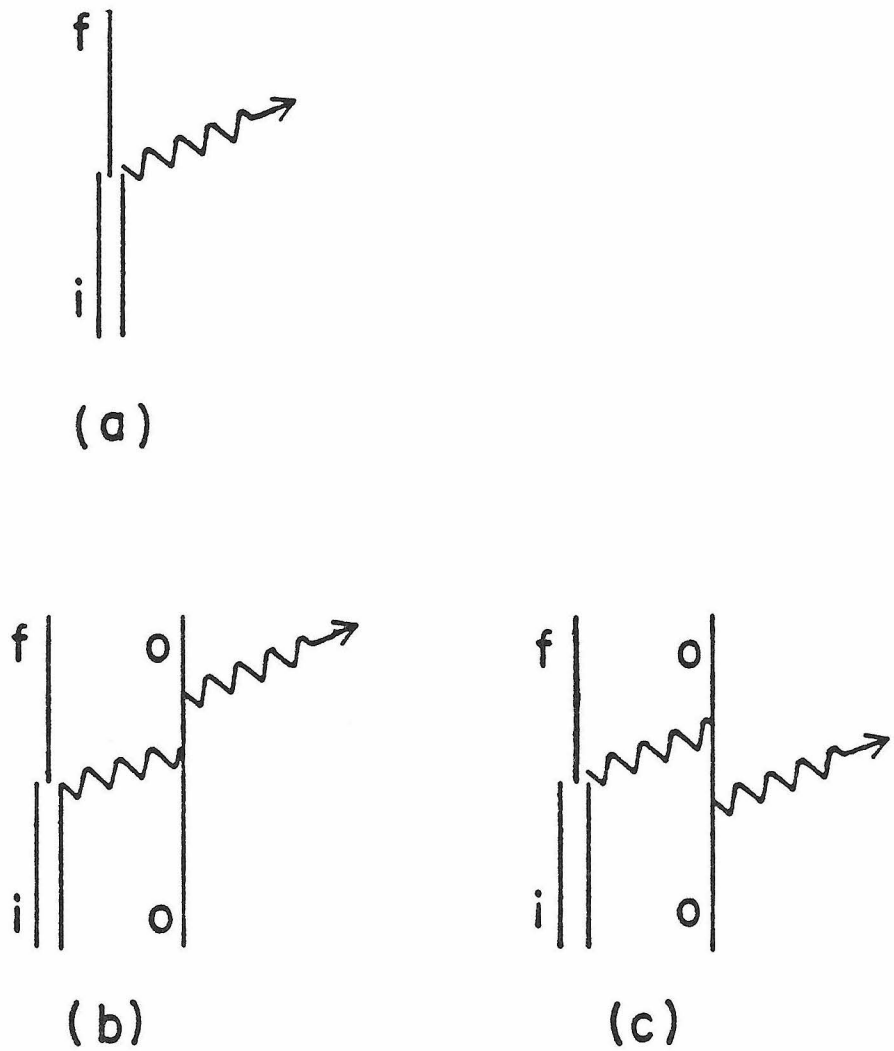

Fig. 1. Diagrams for photon emission in a nuclear transition. The second line of diagrams (b) and (c) represents a bound electron with initial and final state o.

with $\xi = \xi(L'\pi') - \xi(L\pi)$. The quantity measured in angular correlation experiments is thus $\sin(\eta+\xi)$ rather than $\sin\eta$.

The parameters ξ (sometimes referred to as "screening" or "interference" parameters) also enter in Mossbauer absorption studies due to the interference of the scattering processes of Fig. 1b,c following nuclear resonant scattering with the direct scattering of photons by atomic electrons. This results in a "dispersion" term in the γ-ray absorption spectrum, with an attenuation cross section

$$\sigma = \frac{\sigma_o(1 - 2\xi x)}{1 + x^2} + \sigma_e. \tag{1.7}$$

Here σ_o is the nuclear absorption cross section on resonance, x the deviation of photon energy from resonance energy in units of transition half width, and σ_e the total cross section for scattering off atomic electrons. It was in this second connection that studies of final state effects were first made by Hannon and Trammell[24] and Kagan et al.[25].

The phase shifts $\xi(L\pi)$ in general depend upon the multipolarity and energy of the nuclear transition. Goldwire and Hannon[26] have made calculations of phase shifts treating the two processes of virtual internal conversion and virtual Thomson scattering of nuclear radiation off atomic electrons. Rough approximations for the conversion and Thomson phase shifts $\xi_C(L\pi)$ and $\xi_R(L\pi)$ are given[26] by

$$\xi_C(L\pi) \simeq \varepsilon\left[\alpha(L\pi)\sigma_p(L\pi)/(4L + 2)\pi\lambda\!\!\!^{-}_o{}^2\right]^{1/2},$$

$$\xi_R(L\pi) \simeq -\left[\sigma_R(L\pi)/(4L + 2)\pi\lambda\!\!\!^{-}_o{}^2\right]^{1/2}, \tag{1.8}$$

where $\alpha(L\pi)$ is the internal conversion coefficient, σ_p and σ_R are the partial cross sections for the $(L\pi)$ contribution to photoelectric absorption and Thomson scattering, respectively, λ_o is the wavelength of the emitted gamma ray, and ϵ is a real number with absolute value somewhat less than one. Detailed calculations of ξ_C and ξ_R have been made for various multipole transitions at different energies and atomic numbers.

To illustrate the general results of Goldwire and Hannon's calculations, Fig. 2 plots the phase shifts $-[\xi_C(E2) - \xi_C(M1)]$ and $[\xi_R(E2) - \xi_R(M1)]$ between E2 and M1 multipoles as a function of Z, at E = 100 and 200 keV. The Thomson phase shift is relatively insensitive to energy. As indicated, the phase $\xi = \xi_C + \xi_R$ is largest at low energies and for $Z \simeq 60$, and is smaller for high energy, low Z transitions. [A narrow region at Z = 80 also gives a minimum value for ξ due to the cancellation of ξ_C and ξ_R terms.]

As explicitly illustrated by Eq. (1.6), the understanding of final state effects and a precise knowledge of ξ is a prerequisite for the analysis of time-reversal studies in nuclear physics. Aside from this practical aspect, the investigation of these quantum electrodynamical corrections is of course important in its own right. With this motivation a case with a large expected final state phase shift (the 129 keV mixed transition in ^{191}Ir) was selected for a time-reversal experiment based on the correlation (1.2) as a test of the calculations of Goldwire and Hannon. The results of this experiment have in turn motivated a revised calculation of atomic final state phase shifts by Davis et al.[23] which uses a more precise Hartree-Fock treatment of the bound and continuum electron wave functions and includes the so-called "anomalous" scattering contribution to virtual Rayleigh scattering in the calculation of ξ_R.

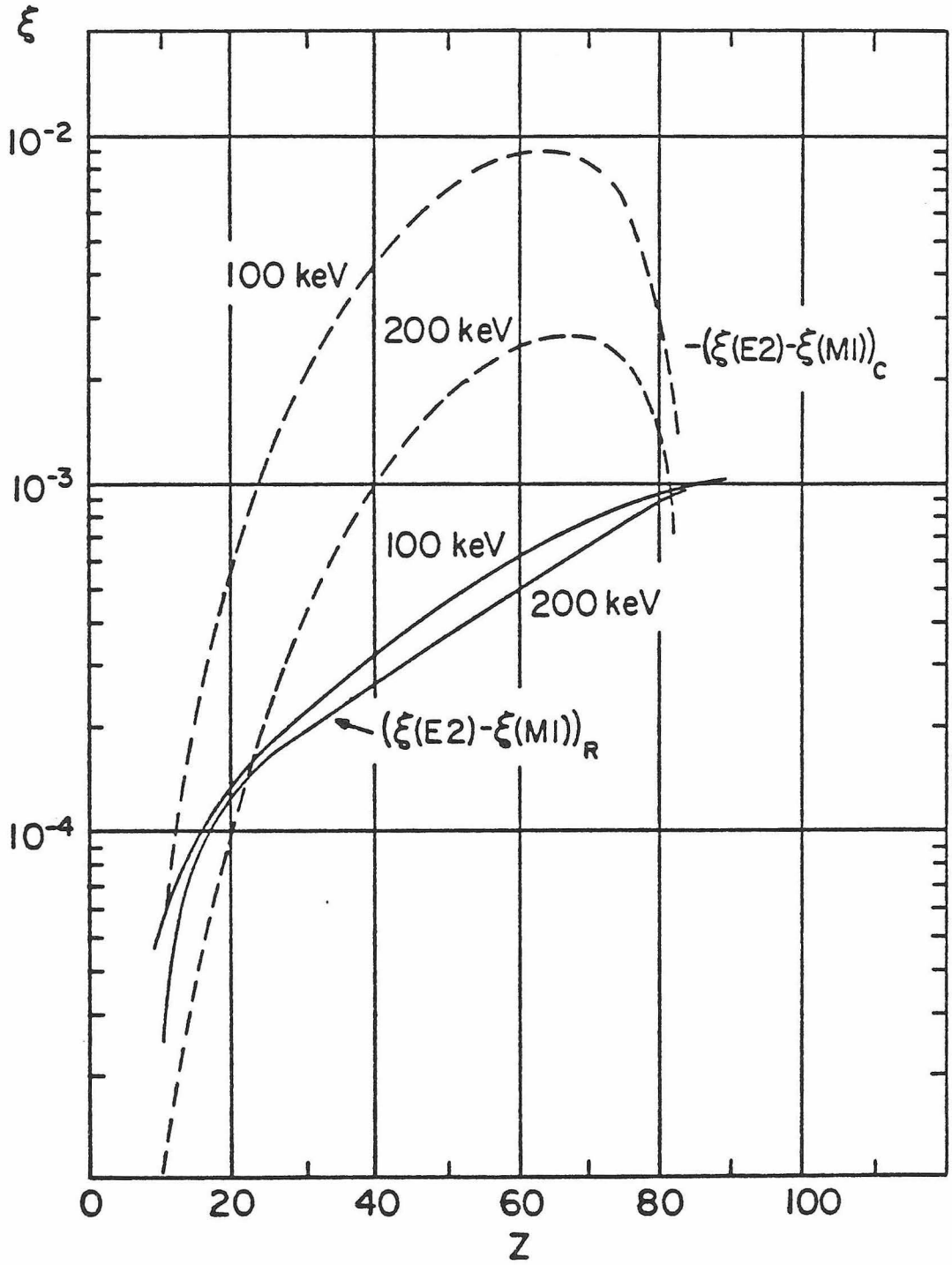

Fig. 2. Phase shifts ξ arising from atomic processes versus atomic number Z. Conversion and scattering phase shifts ξ_C and ξ_R are shown for energies of 100 and 200 keV.

CHAPTER 2

PRINCIPLES OF THE EXPERIMENT

2.1. Angular Distribution from Oriented Nuclei

The angular distribution of gamma radiation emitted from an axially symmetric oriented source may be written as a sum of three terms[19],[27],[28]:

$$W(\theta,\phi) = W_1(\theta) + W_2(\theta,\phi) + W_3(\theta,\phi), \tag{2.1}$$

where θ is the angle between the emission vector $\vec{k}$ and the orientation vector $\vec{J}$, and ϕ is the angle between the linear polarization vector $\vec{E}$ and the $\vec{J}$-$\vec{k}$ plane.

$W_1(\theta)$ is the directional (intensity) distribution of the radiation if linear polarization is not observed, and may be written

$$W_1(\theta) = 1 + \sum_{k=2,4} B_k(I_i) U_k A_k P_k(\cos\theta). \tag{2.2}$$

B_k is the orientation tensor which depends on the initial nuclear spin state I_i and the Boltzmann exponent $(\mu H/I_i kT)$. U_k and A_k are deorientation and angular distribution coefficients respectively, with

$$A_k = F_k(LLI_fI_i) + 2\mathrm{Re}(\delta)F_k(LL'I_fI_i) + |\delta|^2 F_k(L'L'I_fI_i), \tag{2.3}$$

and P_k is the Legendre polynomial of order k. The B_k, U_k, and F_k coefficients are tabulated by Krane[29],[30].

$W_2(\theta,\phi)$ and $W_3(\theta,\phi)$ are the T-even and T-odd linear polarization distribution components, respectively, and are written

$$W_2(\theta,\phi) = \sum_{k=2,4} B_k U_k A_{k2} \left[\frac{(k-2)!}{(k+2)!}\right]^{1/2} P_k^{\,2}(\cos\theta)\cos 2\phi, \tag{2.4}$$

$$W_3(\theta,\phi) = \sum_{k=3} B_k U_k A'_{k2}(-2i)\left[\frac{(k-2)!}{(k+2)!}\right]^{1/2} P_k^{\,2}(\cos\theta)\,\sin 2\phi. \qquad (2.5)$$

The coefficients A_{k2} and A'_{k2} are given by

$$A_{k2} = \frac{-E_p}{2}\Big[-f_k(LL)F_k(LLI_fI_i) + 2|\delta|e^{in\pi}\cos(\eta+\xi)f_k(LL')F_k(LL'I_fI_i)$$
$$+|\delta|^2 f_k(L'L')F_k(L'L'I_fI_i)\Big]/(1+|\delta|^2), \qquad (2.6)$$

$$A'_{k2} = \frac{-E_p}{2}\Big[2i|\delta|e^{in\pi}\sin(\eta+\xi)f_k(LL')F_k(LL'I_fI_i)\Big]/(1+|\delta|^2) \qquad (2.7)$$

for a-linear polarization detection system of efficiency E_p, with

$$f_k(L\,L') = \begin{pmatrix} L & L' & k \\ -1 & -1 & 2 \end{pmatrix}\Big/\begin{pmatrix} L & L' & k \\ 1 & -1 & 0 \end{pmatrix},$$

where L and L' denote the multipolarities 1 and 2 of the mixing, and n = 0 or 1 in the expression $|\delta|e^{in\pi}$.

It is evident that $W_3(\theta,\phi) \propto \left[B_3P_3^{\,2}(\cos\theta)\,\sin 2\phi\right]\sin(\eta+\xi)$ changes sign under a time reversal transformation

$$\vec{k} \to -\vec{k},\ \vec{J} \to -\vec{J},\ \vec{E} \to \vec{E}$$

corresponding to $\theta \to \pi-\theta$, $\phi \to \pi+\phi$, and in fact is proportional to our T-odd correlation $(\langle\vec{J}\rangle \cdot \vec{k} \times \vec{E})$ $(\langle\vec{J}\rangle \cdot \vec{k})$ $(\langle\vec{J}\rangle \cdot \vec{E})$ of (1.3). To measure such a term against the much larger contributions of the W_1 and W_2 distributions it is necessary to compare rates at θ and $\pi - \theta$ (physically amounting to a reversal of the orientation vector $\langle\vec{J}\rangle$). The T-odd contribution is maximized at $\theta_m = 54.7^\circ$ and $\phi_m = 45^\circ$ (for which the $P_2(\cos\theta)$ term of $W_1(\theta)$ and both terms of $W_2(\theta,\phi)$ vanish), and hence the measured "time-reversal" asymmetry is

$$A = \frac{W(\theta_m, \phi_m) - W(\pi-\theta_m, \phi_m)}{W(\theta_m, \phi_m) + W(\pi-\theta_m, \phi_m)}$$

$$= \frac{RQ_3B_3P_3^2(\cos\theta_m)\sin(2\phi_m)E_p\left[|\delta|e^{in\pi}/(1+|\delta|^2)\right]\sin(\eta+\xi)}{1 + SQ_4B_4P_4(\cos\theta_m)|\delta|^2/(1+|\delta|^2)} , \qquad (2.8)$$

where R and S are the spin coefficients

$$R = -(1/\sqrt{30})\, U_3 f_3(LL')F_3(LL'I_fI_i) , \qquad (2.9)$$

$$S = U_4F_4(LL'I_fI_i) . \qquad (2.10)$$

Linear polarization is detected with a Compton polarimeter[19] [which measures the intensity of 90° scattered radiation], and Q_3 and Q_4 denote the solid angle corrections for this polarimeter. The polarimeter efficiency E_p is defined by

$$E_p \equiv \frac{\frac{d\sigma}{d\Omega}(\rho = 90^\circ, \psi = 0^\circ) - \frac{d\sigma}{d\Omega}(\rho = 90^\circ, \psi = 90^\circ)}{\frac{d\sigma}{d\Omega}(\rho = 90^\circ, \psi = 0^\circ) + \frac{d\sigma}{d\Omega}(\rho = 90^\circ, \psi = 90^\circ)} , \qquad (2.11)$$

where $\frac{d\sigma}{d\Omega}$ is the differential cross section for Compton scattering, ρ is the scattering angle and ψ the angle between the initial plane of polarization and the scattering plane. Linearly polarized radiation is preferentially scattered perpendicular to its plane of polarization and E_p is therefore negative.

From Eq. (2.8) it is clear that in order to maximize the sensitivity of A to $\sin(\eta+\xi)$ a large value of B_3, and hence a reasonably large value for the Boltzmann exponential factor $\Delta/T \equiv \mu H/IkT$, is required. Favorable values for the spin coefficients and a mixing ratio δ on the order of unity are also necessary.

CHAPTER 3

EXPERIMENT WITH ^{191}Ir

3.1 The Choice of Nuclear Transition

In order to test the atomic final state calculations of Goldwire and Hannon[26] a transition with a large expected final state phase ξ is necessary. From Fig. 2 we see that this requirement is approximately satisfied for transitions of energy $E < 200$ keV and atomic number $Z > 40$. With this and the aforementioned requirements of large polarizability and mixing in mind, the 129 keV transition in ^{191}Ir was selected for the investigation of atomic final state effects.

The decay scheme of ^{191}Ir is shown in Fig. 3. An isomeric state at 171 keV with 5-sec halflife is populated in the β^- decay of ^{191}Os and cascades down to the 129 keV level. The 41.9 keV γ ray (E3) is internally converted and does not contribute to the spectrum. From NMR measurements the 171 keV state is known to have a magnetic moment $\mu = 5.72 \pm 0.03\ \mu_n$[32], and an internal field for Ir in Fe of -1.481 ± 0.004 MG[31],[32] gives $\Delta \equiv \mu H/Ik = -56.3 \pm 0.3$ mK. A high degree of orientation may therefore be obtained. A relatively large mixing ratio $\mathrm{Re}\,\delta \cong |\delta| e^{i\pi} = -0.399 \pm 0.004$ is reported[33] for the 129 keV transition. With the insertion of spin coefficients into (2.1) - (2.7) the angular distribution for this transition becomes

$$\begin{aligned} W(\theta,\phi) = 1 &+ 0.7300\, B_2 P_2(\cos\theta) + 0.0351\, B_4 P_4(\cos\theta) \\ &+ E_p\left[0.0303\, B_2 P_2^{\,2}(\cos\theta) - 0.00292\, B_4 P_4^{\,2}(\cos\theta)\right]\cos 2\phi \\ &+ E_p\left[0.0365\, B_3 P_3^{\,2}(\cos\theta)\sin 2\phi\right]\sin(\eta+\xi). \end{aligned} \tag{3.1}$$

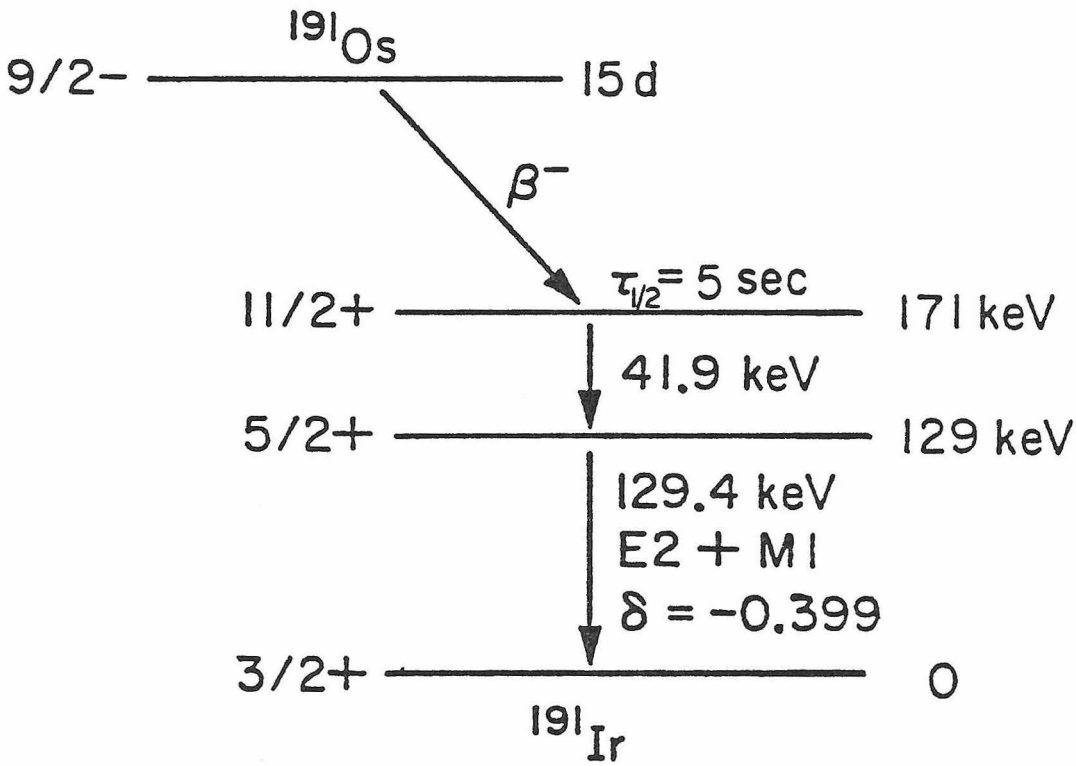

Fig. 3. Decay scheme of ^{191}Os.

3.2 Source Preparation

^{191}Os was produced by neutron capture in a 10 mg, metallic, isotopically enriched sample of ^{190}Os sealed in an evacuated quartz capsule. The sample was alloyed with 300 mg of Fe in an induction furnace in argon atmosphere. The resulting 1 at.% Os(Fe) pellet was then polished to remove surface oxide contamination, and by successive rolling and annealing a thin foil less than 0.025 mm thick was obtained. To assure ourselves of the uniformity of the alloy, narrow strips of foil were scanned with a slit detector. Disks of 0.32 cm diameter were punched, polished with No. 1200 lapping compound, and finally annealed at 800 C in hydrogen atmosphere.

The finished disks, with strengths ranging from 0.5 to 1.0 mCi, were indium-soldered in a horizontal plane to the oxygen-free copper *collar button* of Fig. 4 (in one run a platinum collar button was used to minimize possible magnetostrictive effects) attached to the cooling rod of a dilution refrigerator,[34] and cooled to about 25 mK. A pair of superconducting Helmholtz coils provided (with 5A input current) a 2 kG external field saturating the iron foil. The ^{191}Ir nuclei are polarized via the large magnetic hyperfine interaction experienced by Ir in the Fe host. Because electronic relaxation times are short compared to the 5-sec halflife[32], full nuclear orientation in the 171 keV state was assumed.

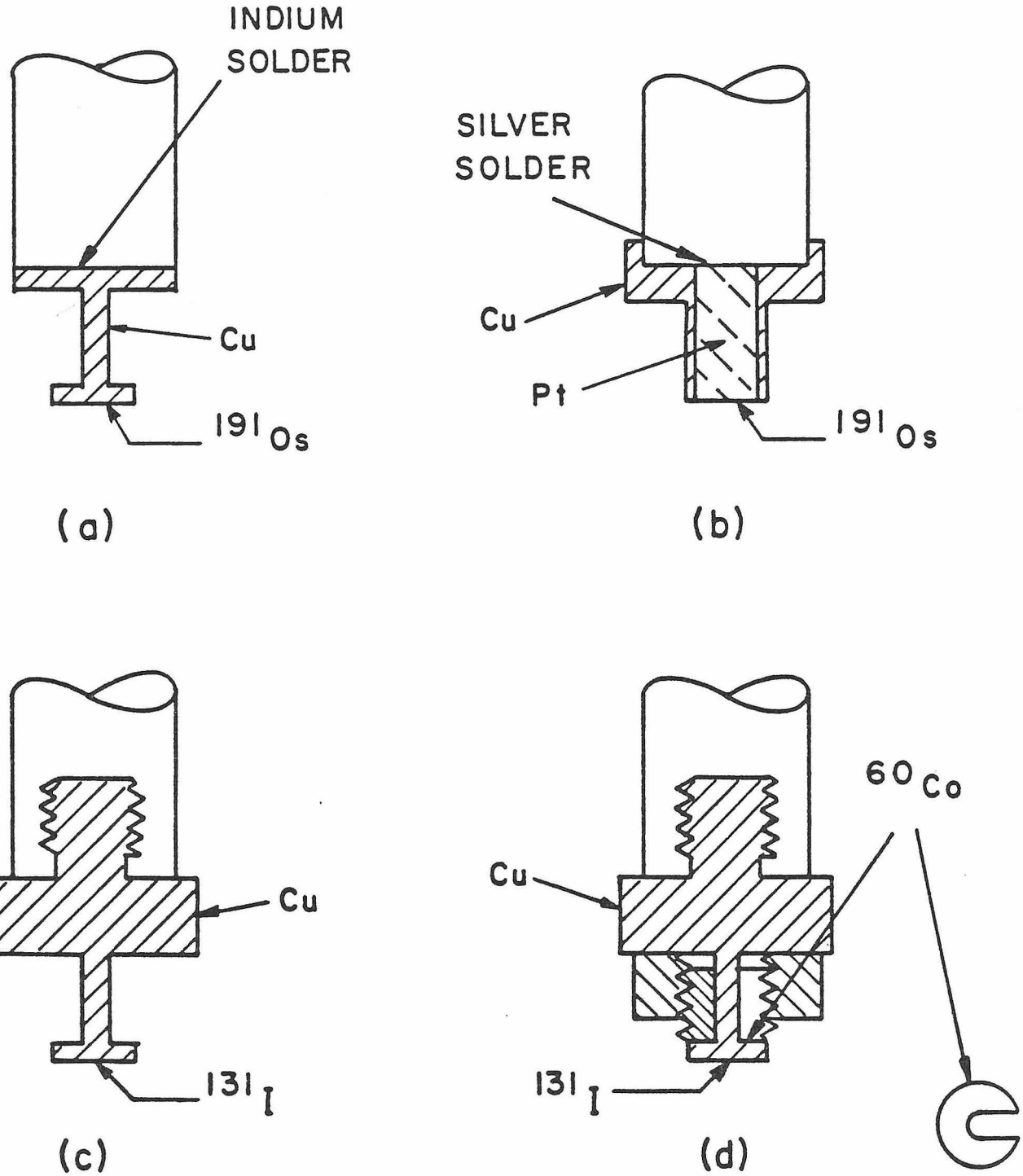

Fig. 4. Source collar buttons used in the ^{191}Ir and ^{131}Xe experiments.

3.3 Experimental Setup

The physical setup of the experiment, similar to that of Ref. 19, is shown in Fig. 5. The source foil is in the horizontal plane in the center of two pairs of superconducting Helmholtz coils which are thermally anchored to the 4K shield of the refrigerator. The Compton polarimeter consists of four NaI(Tl) counters mounted at 90° from each other in a plane about an aluminum scatterer. Gamma rays scattered at 90° from the incident beam are detected. In order to maximize sensitivity to the T-odd term $W_3(\theta,\phi)$, the polarimeter is fixed at an angle $\theta = \theta_m = 54.7^{\circ}$ from the (horizontal) $\vec{H}$ axis. [By convention the quantization axis has been chosen to be that of the externally applied field; for this convention $\Delta = \mu H(\text{hyperfine})/Ik$ is negative and B_3 positive[35].] The four-pronged detector assembly, which is free to rotate through an angle $0 \leq \phi \leq 360^{\circ}$ about its axis of symmetry, is positioned so that NaI counters Nos. 1, 2, 3, and 4 are located at some cyclic permutation of angles $\phi = \phi_m = 45^{\circ}$, 135°, 225°, and 315°. The pedestal supporting the polarimeter may be rotated through an arbitrary angle $0 \leq \psi \leq 360^{\circ}$ about its own axis coincident with the (vertical) axis of cooling rod and source. The four ψ positions corresponding to the axes of the orthogonal coil pairs were designated as N, S, E, and W. A hyperpure germanium (Ge) detector, used to monitor the intensity distribution $W_1(\theta)$ of the source, is supported by a carriage that rolls on a circular track concentric with the pedestal. It was generally positioned at 180° from the polarimeter.

To eliminate magnetic influence on the photomultipliers, each NaI is optically coupled by means of a 30 cm Lucite light pipe to its magnetically shielded phototube. Output from the four photomultipliers is amplified via the usual preamplifier and linear amplifier stages, which provide the input

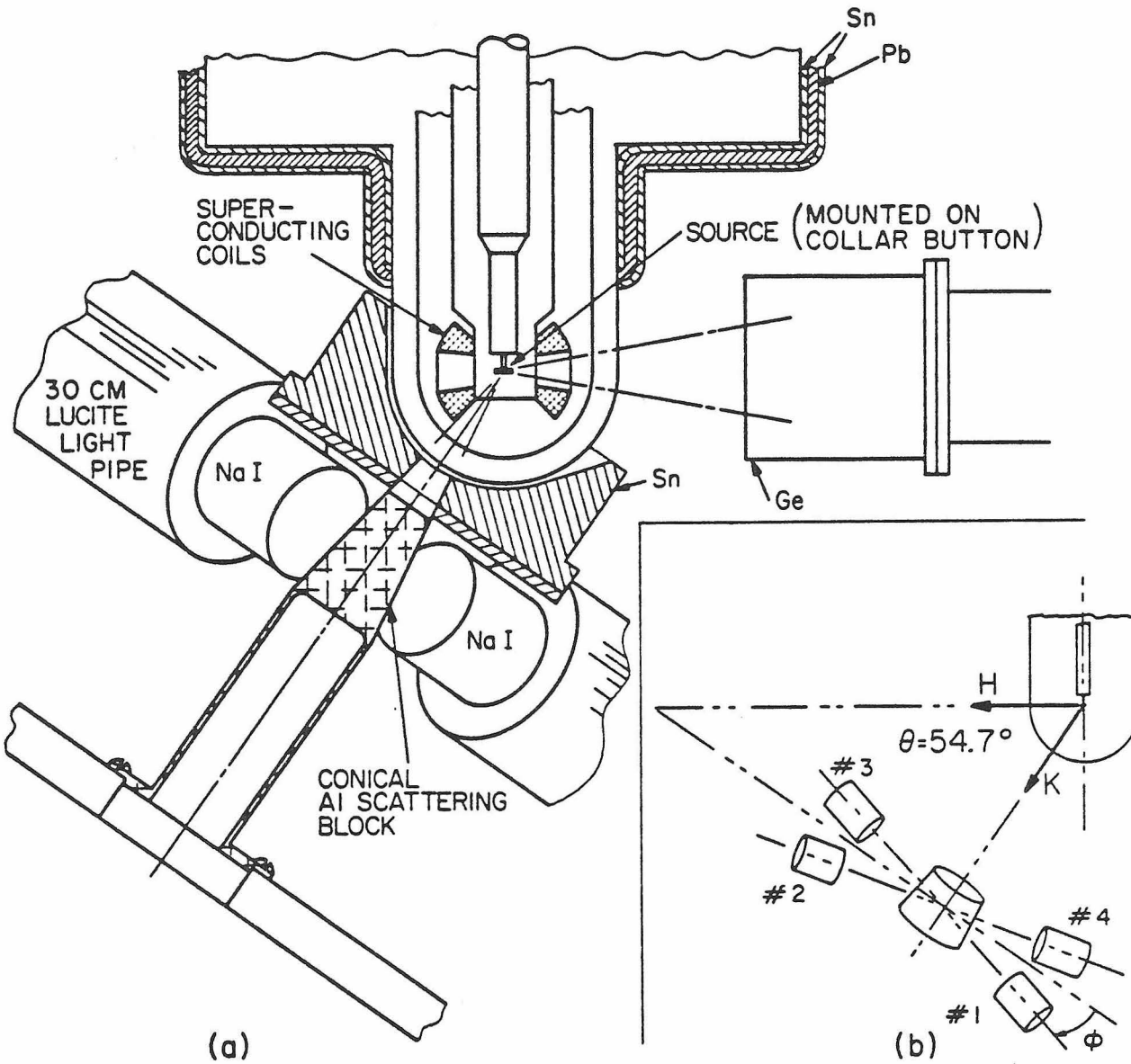

Fig. 5. Diagram showing the polarimeter and its geometry relative to the source and magnet positions. Only two of the four NaI detectors of the polarimeter are shown in the main diagram.

to both the four-input multiplexer/router front end stage of a Northern 1700 multichannel analyzer and to four single channel analyzers. The pulse height spectra of the MCA were recorded on magnetic tape; output from the SCA's were recorded on teletype and paper tape. In practice SCA output was used almost exclusively in data analysis and the pulse height spectra used to monitor detector performance.

"Time-reversal" data were typically acquired in paired sequences of 24 hour runs at opposite ψ positions to cancel out certain systematic effects associated with improperly reversing fields (this will be discussed later in more detail). Source temperature measurements with the Ge detector, to be discussed in the following section, were made at the conclusion of a pair of runs. Pulse height spectra for the Ge detector for these measurements were obtained with the TN1700. The 129 keV photopeak was in addition continuously monitored with a single channel analyzer. Data acquisition was interrupted at 12 and 24 hour intervals to fill the liquid nitrogen and helium reservoirs of the refrigerator.

3.4 Source Temperature Determination

To determine the source temperature, and hence the degree of nuclear orientation (i.e. the B_k coefficients appearing in (2.2) - (2.8)), the following procedures were adopted. After each pair of "time-reversal" asymmetry runs the directional distribution of (2.2) for the 129 keV γ ray in the plane of the source was measured with the Ge detector. As shown in Fig. 6 this distribution is very elongated along the axis of the applied field. By measuring peak count rates in the Ge pulse height spectra with the external magnetic field applied first parallel (0°) and then perpendicular (90°) to the axis of the detector a precise determination of the anisotropy ratio

$$\frac{W_1(\theta = 0^\circ)}{W_1(\theta = 90^\circ)} = \frac{1 + \sum_{k=2,4} Q_k B_k U_k A_k P_k(\cos 0^\circ)}{1 + \sum_{k=2,4} Q_k B_k U_k A_k P_k(\cos 90^\circ)} \qquad (3.2)$$

could be made, where solid angle corrections Q_k[36] for the detector have been inserted. The orientation coefficients

$$B_k = \left[(2I + 1)(2k + 1)\right]^{1/2} \frac{\sum_{m=-I}^{I} (-)^{I+m} \begin{pmatrix} I & I & k \\ -m & m & 0 \end{pmatrix} e^{m\Delta/T}}{\sum_{m=-I}^{I} e^{m\Delta/T}},$$

and thus the temperature T, could in principle be calculated were it not for the partial nonalignment of the Ir nuclei in Fe[37]. An independent determination of temperature was therefore necessary. After completion of an experiment a ^{60}Co(Fe) foil was indium-soldered to the ^{191}Os(Fe) source and a calibration of the observed 129 keV anisotropy as a function of source temperature obtained from the known[38],[39] distribution of the ^{60}Co(Fe) was made.

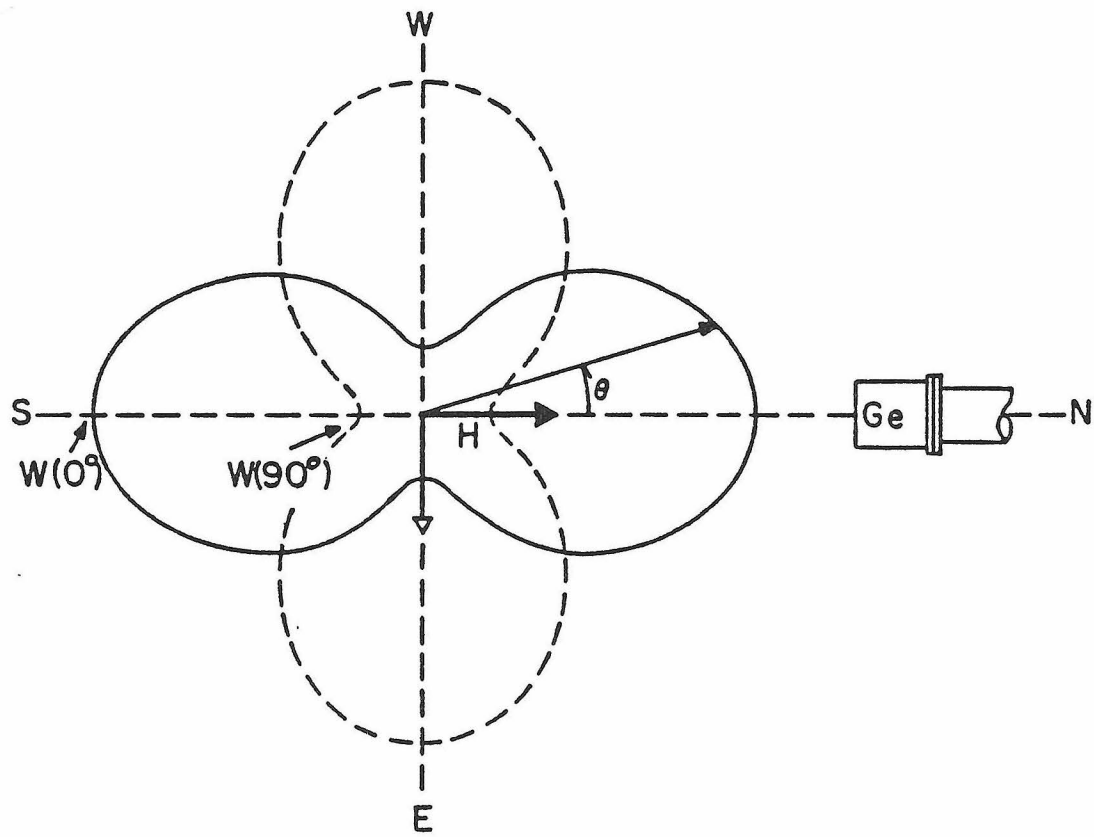

Fig. 6. Polar plot of the directional distribution $W(\theta)$ of the 129 keV line.

[The Co(Fe) sources were prepared as in Ref. 19, with the exception that the disk surfaces were treated by polishing with No. 1200 lapping compound rather than etched with HCl.] The partial nonalignment of ^{191}Ir was empirically treated as being the result of one or both of two possible phenomena: (1) microscopic inhomogeneities resulting in a fraction of the nuclei experiencing a small or vanishing field while the remainder sees the full hyperfine field, and (2) an overall reduction in hyperfine field saturation experienced by all nuclei. A two-parameter fit (see Fig. 7) of temperature to the 129 keV ratio $W_1'(0)/W_1'(90)$, with

$$W_1'(\theta) = 1 + \sum_{k=2,4} Q_k f_a B_k(f_s\Delta/T) U_k A_k P_k(\cos\theta)$$

$$= 1 + 0.726\ f_a B_2(f_s\Delta/T) P_2 + 0.0344\ f_a B_4(f_s\Delta/T) P_4, \qquad (3.3)$$

yielded the free parameters f_a (the fraction of properly sited Ir nuclei experiencing the 1.481 MG field) and f_s (the degree of magnetic saturation). It was found that $f_a = 0.940 \pm 0.005$ and $f_s = 0.99 \pm 0.02$ for all but one source, which suffered from an unexplained reduction in magnetic saturation with $f_a = 0.957 \pm 0.005$ and $f_s = 0.75 \pm 0.02$.

The anisotropy measurements $W_1(0^\circ)/W_1(90^\circ)$ obtained with the Ge detector for each experiment were then reanalyzed in terms of this effective distribution $W_1'(\theta)$ which replaces $B_{2,4}(\Delta/T)$ by $f_a B_{2,4}(f_s\Delta/T)$. In this manner the source temperature as a function of time was determined for each experiment, and an effective third order polarization coefficient $B_3(\text{eff}) = f_a B_3(f_s\Delta/T)$ was calculated. [Other models could have been chosen to explain the incomplete polarization of ^{191}Ir(Fe). For example, one model which was used to explain a much larger degree of nonalignment in ^{191}Ir (source preparation is

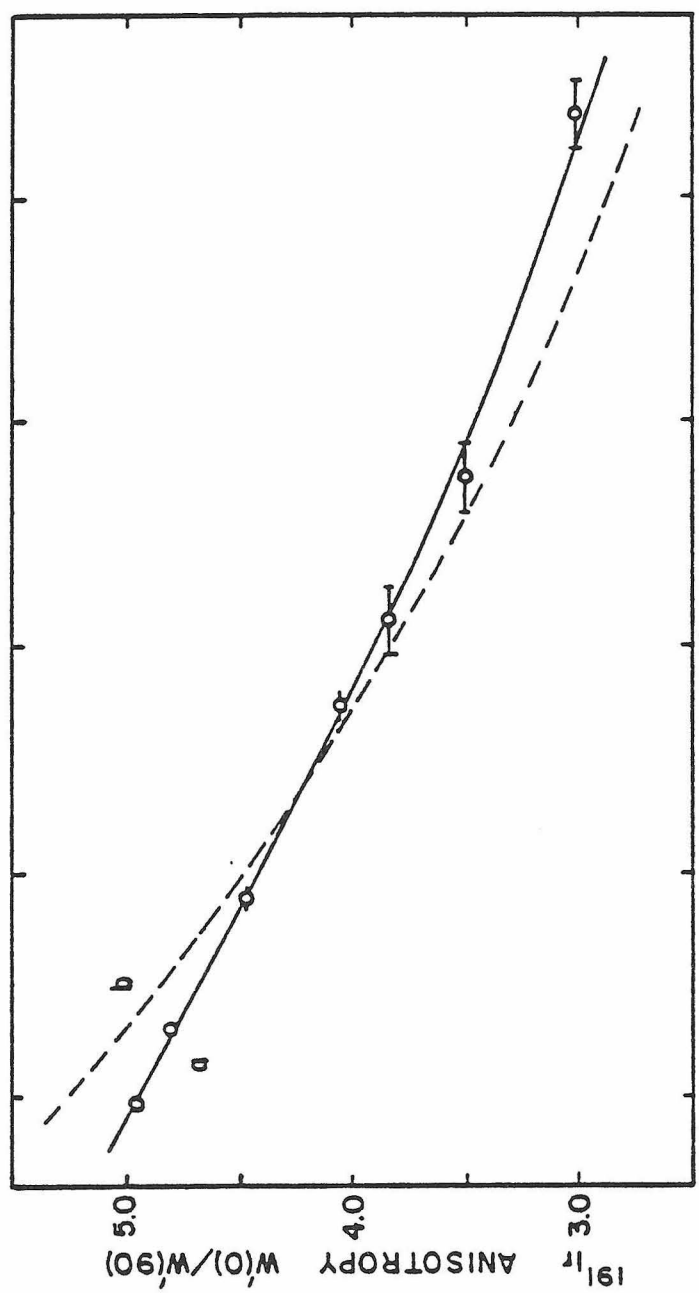

Fig. 7. Two-parameter fit of observed ^{191}Ir anisotropy $W'(0°)/W'(90°)$, with $W'(\theta) = 1 + \sum_{2,4} Q_k f_a B_k (f_s \Delta/T) U_k A_k P_k(\cos\theta)$, to ^{60}Co-determined temperature T. Curve a is the best fit with parameters $f_a = 0.94$ and $f_s = 0.99$. Curve b represents the best fit if it is assumed that $f_a = 1.0$.

apparently critical) speaks of a "cone angle" Θ defined by the polarization vectors of the Ir nuclei about the applied field vector[37]. Since our parameters assume values near unity, however, the calculation for B_3 is quite model independent.]

$W(\theta = 0^{\circ})$ was continuously monitored with the Ge detector concurrent with the "time-reversal" data acquisition as a check on temperature stability.

3.5 Revisions in the Polarimeter

The first experiment used the polarimeter configuration of Fig. 8a (polarimeter 1). A cadmium-lined lead cup covering the refrigerator tail piece shields the NaI detectors from direct radiation from the source. Small exit windows collimate the γ rays impinging upon scatterer and Ge detector. Also shown is the resulting spectrum for a single NaI counter. As is indicated, a large proportion of low energy Ir (and in addition Pb) x rays significantly dilute the spectrum.

Numerous changes in the polarimeter were made for subsequent runs. The lead shielding previously affixed to the tail piece of the dilution refrigerator was replaced by a tin ring attached to the polarimeter itself. This had the dual effect of maintaining a fixed collimator-to-scattering-block geometry and also of reducing the Pb x rays. The remaining lead around the refrigerator was sandwiched between 0.16 cm tin. The NaI crystals were individually wrapped with additional tin to reduce the contribution of backscattered radiation. Finally, a 0.09 cm thick tin absorber was placed in front of the aluminum scattering block to preferentially attenuate the Ir x rays with respect to the 129 keV γ ray. Although this resulted in a 40% reduction in the gamma count rate, with a corresponding 23% reduction in statistics, a factor of two increased detector polarization efficiency was realized. Fig. 8b shows the revised polarimeter (polarimeter 2) and its Compton-scattered spectrum.

Alignment of source, superconducting coils, and polarimeter was carefully maintained to within 0.02 mm, typically. Refrigerator movement with respect to the collimator was monitored by a position-sensitive indicator attached to the polarimeter, and if necessary was corrected with the three aluminum struts which fixed the refrigerator to the rails supporting the polarimeter.

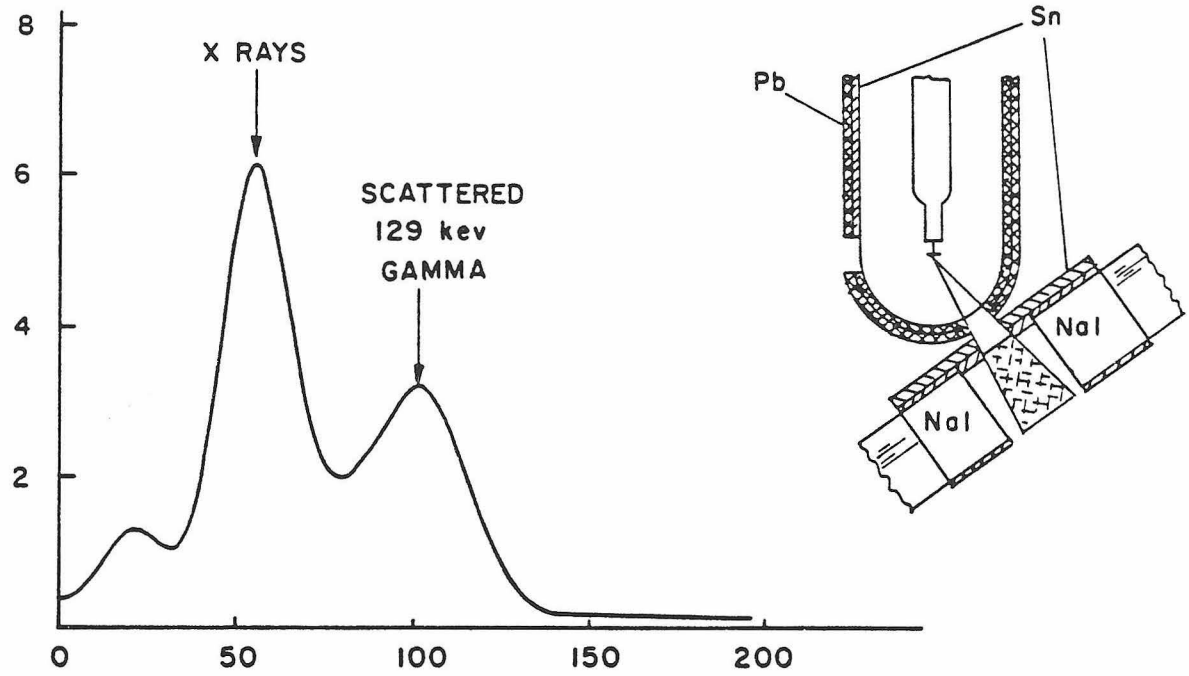

(1)

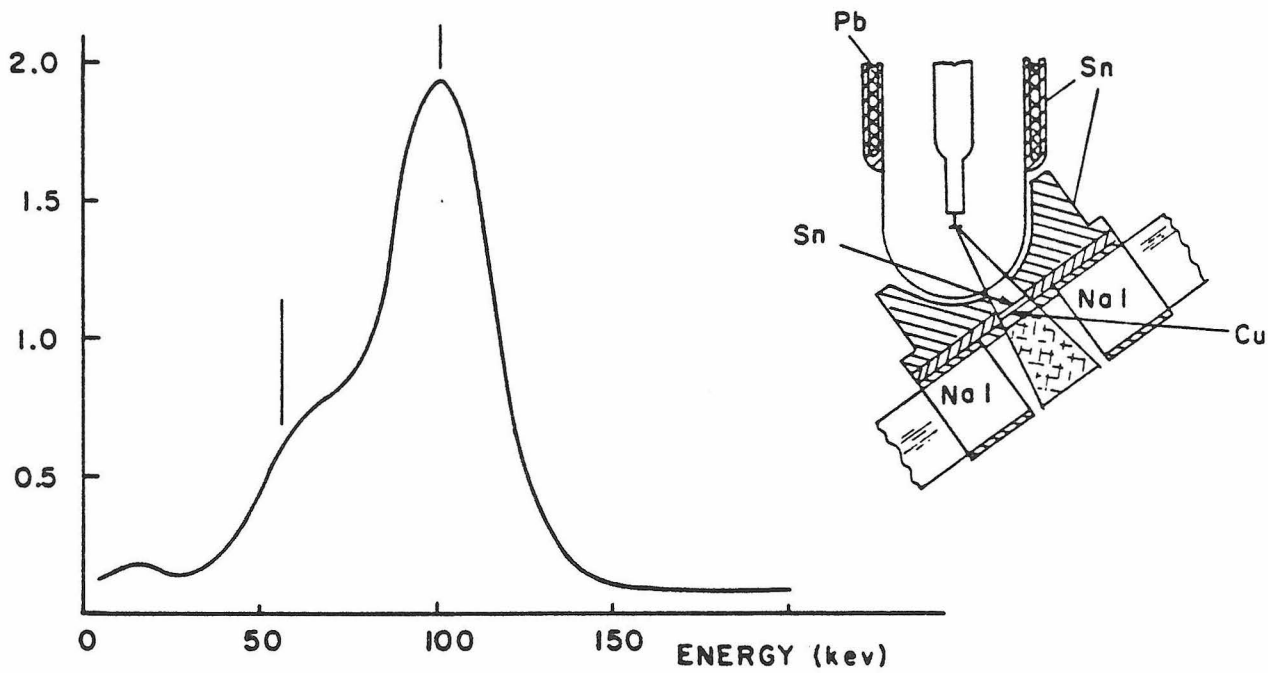

(2)

Fig. 8. Versions 1 and 2 of polarimeter shielding, with the resulting energy spectra for a single NaI detector.

3.6 Polarimeter Efficiency Determination

(i) Measurement from oriented ^{191}Ir

The efficiency E_p of the polarimeter for detecting linearly polarized radiation was determined from a measurement of the asymmetry

$$A_p'(\theta) = \frac{W'(\theta,\ \phi = 0^\circ) - W'(\theta,\ \phi = 90^\circ)}{W'(\theta,\ \phi = 0^\circ) + W'(\theta,\ \phi = 90^\circ)} \tag{3.4}$$

at $\theta = 54.7^\circ$ and 90°. The rates $W'(\theta,\phi)$ represent the total counts in a single channel window extending from 30 to 150 keV and including the scattered ^{191}Ir peak, (unresolved) scattered Ir x rays, and background, as shown in Fig. 9a. The x rays contribute no asymmetry to A_p' but their presence dilutes the measured effect, so that

$$\begin{aligned} E_p'(\text{measured}) &= E_p(129\ \text{keV}) \times N_\gamma/(N_x + N_\gamma) \\ &= E_p(129)/(1 + N_x/N_\gamma) \\ &= E_p(129)/(1 + g), \end{aligned} \tag{3.5}$$

with $g \equiv N_x/N_\gamma$, the ratio of scattered x rays to scattered 129 keV gamma rays in the NaI spectrum. The factor g is common to both the polarization efficiency measurement (at $\theta = 54.7^\circ$) and the measured "time-reversal" asymmetry A', and does not influence the result for $\sin(\eta+\xi)$ since

$$\sin(\eta+\xi) \propto A/E_p = A'(1 + g)/E_p'\ (1 + g) = A'/E_p' \ . \tag{3.6}$$

We may therefore speak of an effective polarization efficiency E_p, ignore the factor $(1 + g)$ and drop the primes.

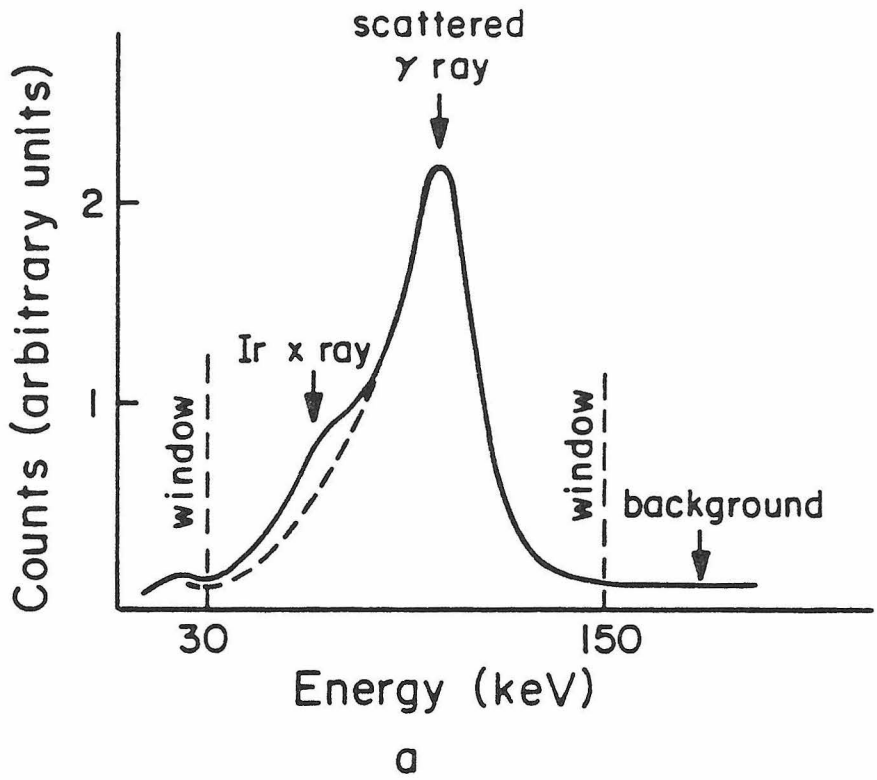

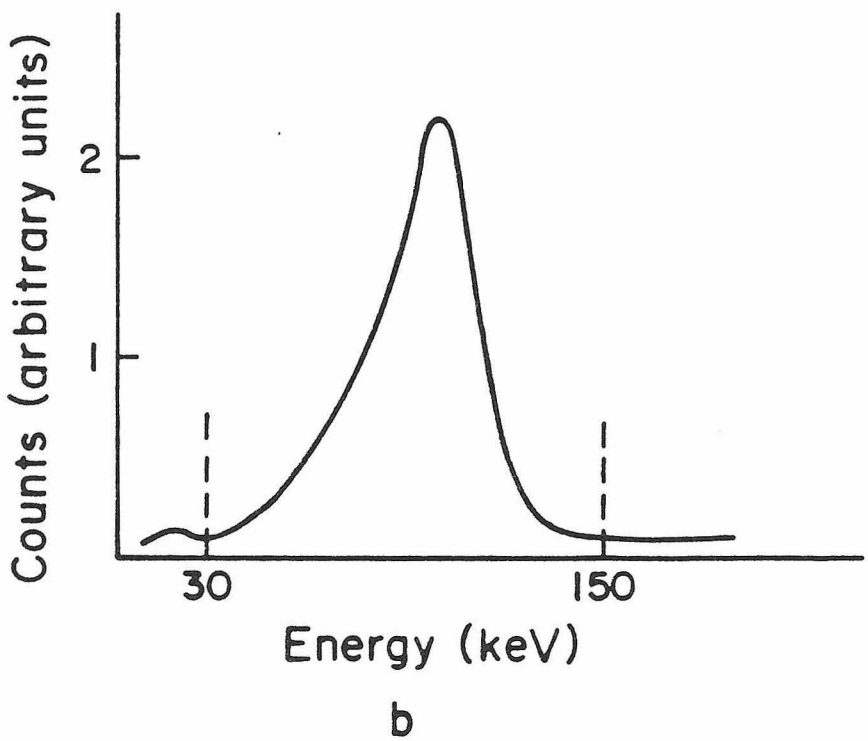

Fig. 9. NaI spectra of the Compton-scattered 129 and 122 keV lines of ^{191}Ir (a) and ^{57}Fe (b). SCA windows are indicated.

The background in the polarimeter spectrum consists not only of high energy radiation from the environment entering the NaI detectors (amounting typically to 1 or 2% of the entire spectrum) but also, unfortunately, of radiation from the source which enters the detectors directly through the shielding. This direct radiation is composed of a small amount of the 129 keV γ ray (contributing a few percent to the total spectrum) and in the case of two later runs a sizeable amount of 300 keV radiation from ^{192}Ir contaminants in the source. Because of asymmetric absorption by the superconducting coils and the anisotropic emission of oriented ^{191}Ir and ^{192}Ir, such direct radiation will exhibit its own asymmetry in the measurement of A_p', and its effect must be deconvolved to obtain a "true" efficiency asymmetry A_p for the scattered 129 keV line. Background corrections (discussed in Appendix A) may be deduced from efficiency measurements at 4K. Because of the uncertainty in the relative amounts of contributing radiation, however, these corrections substantially limit the accuracy of the efficiency determination.

The background does not contribute to the time-reversal asymmetry but will dilute the measured value in the same manner as the x rays, so that

$$\sin(\eta+\xi) \propto A/E_p = A'(1 + f)/E_p , \tag{3.7}$$

with A' the measured asymmetry and the unprimed variables referring to background-corrected values. The parameter f is defined as the ratio of background to the scattered 129 keV line (plus unresolved x rays).

From (3.1) and (3.4) we obtain for the polarization efficiency asymmetries

$$A_p(\theta= 54.7^\circ) = E_p \frac{0.0606\ Q_2 f_a B_2 - 0.0195\ Q_4 f_a B_4}{1 - 0.0136\ Q_4 f_a B_4} , \tag{3.8}$$

$$A_p(\theta = 90^\circ) = E_p \frac{0.0909\, Q_2 f_a B_2 + 0.0219\, Q_4 f_a B_4}{1 - 0.365\, Q_2 f_a B_2 + 0.0132\, Q_4 f_a B_4} . \qquad (3.9)$$

The solid angle corrections Q_k for the polarimeter are $Q_2 = 0.982$, $Q_3 = 0.963$, and $Q_4 = 0.940$[19]. To measure $A_p'(\theta = 54.7^\circ)$ the polarimeter was physically rotated to four positions corresponding to $\phi = 0^\circ$, 90°, 180°, and 270°, and A_p' was taken to be

$$A_p'(\theta = 54.7^\circ) = \frac{\sum_{NaI=1}^{4} W_i'(\phi = 0) + W_i'(180) - W_i'(90) - W_i'(270)}{\sum_{NaI=1}^{4} W_i'(0) + W_i'(180) + W_i'(90) + W_i'(270)} . \qquad (3.10)$$

This averaging over the four detectors and four positions served to cancel out small geometric effects.

Efficiency measurements for polarimeter 1 were made at T = 21.5 mK, with $f_a B_2 = 1.58$, $f_a B_4 = 1.04$, and $A_p(\theta = 54.7) = (0.0760 \pm 0.0038)\, E_p$. (This proportionality constant relating A_p to E_p is quite sensitive to a deviation in mixing ratio $\delta = -0.399 \pm 0.004$; hence the 5% uncertainty.) From a raw asymmetry $A_p' = -0.0172 \pm 0.0004$, a background-corrected value $A_p = -0.0163 \pm 0.0016$ was deduced, yielding an efficiency $E_p = -0.215 \pm 0.023$.

For efficiency measurements at $\theta = 90^\circ$ the polarimeter may be left stationary while the field is rotated 90°. However, at $\theta = 90^\circ$ the 129 keV γ-ray emission is reduced (the reduction factor is the denominator D in (3.9)) relative to emission at $\theta = 54.7^\circ$ while the x-ray intensity remains the same. The difference in the proportion of x rays in the 90° spectrum must therefore be corrected for. This amounts to replacing the factor (1 + g) in (3.6) by (1 + g/D). The ratio g was determined by subtracting (see Fig. 9) from the ^{191}Ir spectrum a spectrum obtained with a ^{57}Co source (consisting of

a 122 keV line and no unresolved x rays). For the first run using polarimeter 1 a value of g = 1.08 ±0.15 was found. For subsequent runs with polarimeter 2, g = 0.07 ±0.03.

From a raw asymmetry $A_p'(\theta = 90^\circ) = -0.0412 \pm 0.0010$, a corrected asymmetry $A_p(90^\circ) = -0.0450 \pm 0.0040$ was obtained for polarimeter 1, giving $E_p(90^\circ) = -0.122 \pm 0.011$. Applying an x-ray correction factor $(1+g/D)/(1+g) = 1.65 \pm 0.05$ gives $E_p = -0.201 \pm 0.019$, in fair agreement with the measurement at $\theta = 54.7^\circ$. For the first polarimeter, then, a value $E_p = -0.21 \pm 0.02$ was finally adopted.

Similar measurements were made with polarimeter 2. From the raw asymmetries $A_p'(54.7^\circ) = -0.0333 \pm 0.0004$ and $A_p'(90^\circ) = -0.112 \pm 0.001$, background-corrected asymmetries $A_p(54.7^\circ) = -0.316 \pm 0.0025$ and $A_p(90^\circ) = -0.137 \pm 0.010$ were deduced. The 54.7° data were taken at T = 24.2 mK, with $f_a B_2 = 1.54$ and $f_a B_4 = 0.99$, for which we obtain from A_p an efficiency $E_p = -0.423 \pm 0.038$. The 90° data were obtained at T = 25.3 mK, with $f_a B_2 = 1.52$ and $f_a B_4 = 0.99$. Applying a 1.07 ±0.03 correction factor for x rays then gives $E_p = -0.438 \pm 0.036$ for the 90° measurement.

(ii) Measurement from oriented ^{57}Co

The accuracy of the polarimeter efficiency measurements using ^{191}Ir suffer from the small proportionality coefficient relating the measured asymmetry to E_p, the sensitivity of this coefficient to δ, and the sizeable background corrections required. To decrease the uncertainty of E_p the efficiency of the new polarimeter was also measured using the 122 and 136 keV transitions in ^{57}Fe from the decay of oriented ^{57}Co. This source has the advantage of having a large measurable asymmetry A_p, no unresolved x rays,

and no high energy lines from ^{191}Ir contaminants. Corrections for asymmetric background are negligible.

Assuming an intensity ratio of 89:11 between the 122 and 136 keV lines we have for the efficiency asymmetries[19]

$$A_p(\theta = 54.7^\circ) = E_p \frac{0.2866\ B_2 + 0.0179\ B_4}{1 + 0.01253\ B_4}\ , \tag{3.11}$$

$$A_p(\theta = 90^\circ) = E_p \frac{0.4298\ B_2 - 0.0201\ B_4}{1 - 0.0289\ B_2 - 0.0120\ B_4}\ . \tag{3.12}$$

From a measured value $A_p(54.7^\circ) = -0.0986 \pm 0.0025$ at 18 mK we obtain $E_p = -0.471 \pm 0.012$. Measurements at $\theta = 90^\circ$ gave $A_p(90^\circ) = -0.149 \pm 0.004$ and $E_p = -0.466 \pm 0.012$. An averaged value $E_p = -0.468 \pm 0.010$ was adopted. [For interest this may be compared to a Monte Carlo calculation yielding $E_p = -0.448 \pm 0.007$. This calculation is a refined version of the Monte Carlo program of Ref. 19 and Ref. 35, attempting to accurately reproduce the geometry of the physical polarimeter. The "error" in this value represents the standard deviation of n runs divided by $\sqrt{n}$.] This efficiency represents the "true" polarimeter efficiency for a 122 (or 129) keV line with no dilution from x rays. To be related to our effective ^{191}Ir efficiency it must be scaled by a factor $(1 + g)^{-1}$, with $g = 0.07 \pm 0.03$. We then obtain $E_p = -0.437 \pm 0.015$. Combining this result with the ^{191}Ir measurements yields for the efficiency of polarimeter 2, $E_p = -0.435 \pm 0.015$.

3.7 Measurement of the "Time-Reversal" Asymmetry

The experimental setup for the time-reversal runs is that of Fig. 5, with the polarimeter oriented at $\theta = \theta_m = 54.7^\circ$ and $\phi = \phi_m = 45^\circ$. The asymmetry

$$A = \frac{W(\theta_m,\phi_m) - W(\pi-\theta_m,\phi_m)}{W(\theta_m,\phi_m) + W(\pi-\theta_m,\phi_m)}$$

[Eq. (2.8)] is measured by comparing polarimeter count rates for applied fields of opposite polarity ($\vec{H}$ and $-\vec{H}$). Data were acquired for all four (N, S, E, and W) ψ polarimeter positions, typically in pairs of 24 hour runs at opposite positions (N and S, and E and W). The orienting field of the appropriate superconducting coil pair was reversed ($\theta \rightarrow \pi-\theta$) by inverting the input to the voltage-controlled current supply driving the coils. The input switching waveform, shown in Fig. 10, is controlled by a master timer. At time $t = 0$ data accumulation is stopped and field switching is initiated, as well as a dead time. The latter is set for a time interval t_2 which was generally chosen to be 1 or 2 min. A ramp time t_1 of 25 sec was used for the switching waveform. At the end of the dead time the count gates are opened for the next counting period. In this manner data of alternate-polarity fields were acquired during the t_3 counting periods for 10-min intervals. The driving current was symmetrical about zero to one part in 1000.

The "time-reversal" asymmetry for the ith NaI counter for a pair of (+, -) field counting rates is

$$A_i' = \frac{N_i(+) - N_i(-)}{N_i(+) + N_i(-)}$$

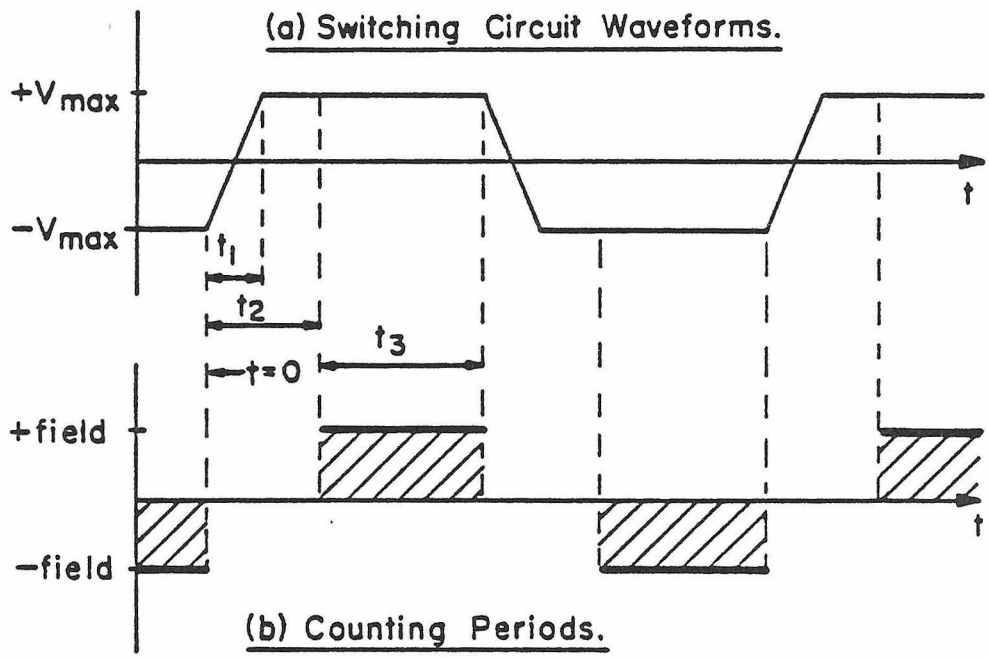

Fig. 10. Magnet switching waveforms and counting periods.

$$= \frac{W_i'(\theta_m, \phi_i) - W_i'(\pi - \theta_m, \phi_i)}{W_i'(\theta_m, \phi_i) + W_i'(\pi - \theta_m, \phi_i)},$$

$$= (-)^{i+1} \frac{W'(\theta_m, \phi_m) - W'(\pi - \theta_m, \phi_m)}{W'(\theta_m, \phi_m) + W'(\pi - \theta_m, \phi_m)}, \qquad (3.13)$$

where the W_i' again refer to the total integrated count rate in the window of Fig. 9, corrected for decay (half-life = 15.4 days), and $\phi_i = 45^\circ$, 135°, 225°, and 315° for i = 1 to 4. In actuality every run was compared to the average of the preceding and following runs in order to eliminate the influence of first order temperature and count rate drifts. The series A_i' were combined and averaged over detectors, adjusting for the signs of detectors 2 and 4 which view opposite polarization patterns relative to detectors 1 and 3 ($W(\theta,\phi) \propto \sin 2\phi_i$). Additionally the asymmetry[40]

$$A' = \frac{1}{8}\left[\frac{M_1N_2M_3N_4}{N_1M_2N_3M_4} - 1\right]$$

was computed for each pair of (+,-) runs, where M_i and N_i refer to (+) and (-) count rates, respectively, for the ith counter. Fortunately count rates proved to be quite stable and the two procedures for computing A' yielded nearly identical results. For all runs (except for a few instances when the electronics failed) the normalized χ^2 was approximately equal to 1; hence the statistical error $\Delta A'$ was equal to that computed from the standard deviation of the distribution of A's. The resulting weighted average A' is the effective asymmetry of (3.7) and may be related to the "true" asymmetry A of (2.8) by multiplying by the background-correction factor (1 + f).

3.8 Results

(i) Results with polarimeter 1

All told four independent measurements with ^{191}Ir were undertaken. Results for the initial experiment with polarimeter 1 are summarized in Table I. The source was a 0.013 mm thick ^{191}Os(Fe) foil indium-soldered to the copper collar button of the refrigerator's cooling rod (Fig. 4a). Data were acquired in series of runs successively for the east, west, north, and south ψ orientations of the polarimeter. Raw asymmetries for the 33 consecutive runs, each of approximately 12 hour duration, are plotted in Fig. 11. A background correction factor $(1 + f) = 1.03 \pm 0.02$ was applied to obtain the corrected asymmetry A, from which $\sin(\eta+\xi)$ was determined via (2.8):

$$\sin(\eta+\xi) = A \frac{1 + SQ_4 f_a B_4 P_4(\cos 54.7^o)|\delta|^2/(1 + |\delta|^2)}{R\, Q_3 f_a B_3 P_3^2(\cos 54.7^o) E_p[|\delta| e^{i\pi}/(1 + |\delta|^2)]} \tag{3.15}$$

$$= A \frac{1 - (0.0128 \pm 0.0002)\, f_a B_4}{(0.203 \pm 0.001)\, f_a B_3 E_p} \quad . \tag{3.16}$$

To obtain (3.16) we have substituted $|\delta| e^{i\pi} = -0.399 \pm 0.004$, $Q_3 = 0.963$, $Q_4 = 0.940$, and numerical values for the spin coefficients $R = -0.1061$ and $S = 0.2556$. The polarization efficiency was $E_p = -0.21 \pm 0.02$ for polarimeter 1. From a corrected asymmetry $A = (2.60 \pm 0.13) \times 10^{-4}$ and a mean third order polarization coefficient $f_a \langle B_3 \rangle = 1.35 \pm 0.03$, we then determined $\sin(\eta+\xi) = (-4.46 \pm 0.48) \times 10^{-3}$.

Also included in Table I are the results of a control experiment at 4K. The asymmetries A' for the 23 runs are plotted in Fig. 12. The consistency

Table I. Results of Experiment No. 1.

Polarimeter Orientation	Temperature T(mK)	Polarization $f_a\langle B_3\rangle$	Raw Asymmetry $A'(10^{-4})$	Corrected[a] Asymmetry $A\ (10^{-4})$	Phase $(\eta+\xi)$ (10^{-3})
E(weighted average)	26.7	1.30	2.56(21)	2.64(22)[b]	-4.70(39)[b]
W	25.1	1.33	2.48(21)	2.55(22)	-4.44(38)
N	22.4	1.37	2.21(22)	2.28(23)	-3.85(39)
S	20.7	1.40	2.85(22)	2.94(23)	-4.86(38)
Weighted Average of N,S,E,W	24	1.35(3)	2.52(11)	2.60(13)[c]	-4.46(48)[d]
Control Runs					
N	4K	0.0	0.44(38)		
S			-0.31(29)		
E			0.12(41)		
W			0.36(34)		
Weighted Average of N,S,E,W			0.09(17)		

Polarization efficiency $E_p = -0.21 \pm 0.02$.

χ^2 per 32 degrees of freedom = 1.15.

a) $A = A'(1 + f) = A'(1.03 \pm 0.02)$.
b) "Error" is the propagated statistical error of A'.
c) Error includes (1 + f) uncertainty.
d) Includes errors of (1 + f), $f_a\langle B_3\rangle$, and E_p.

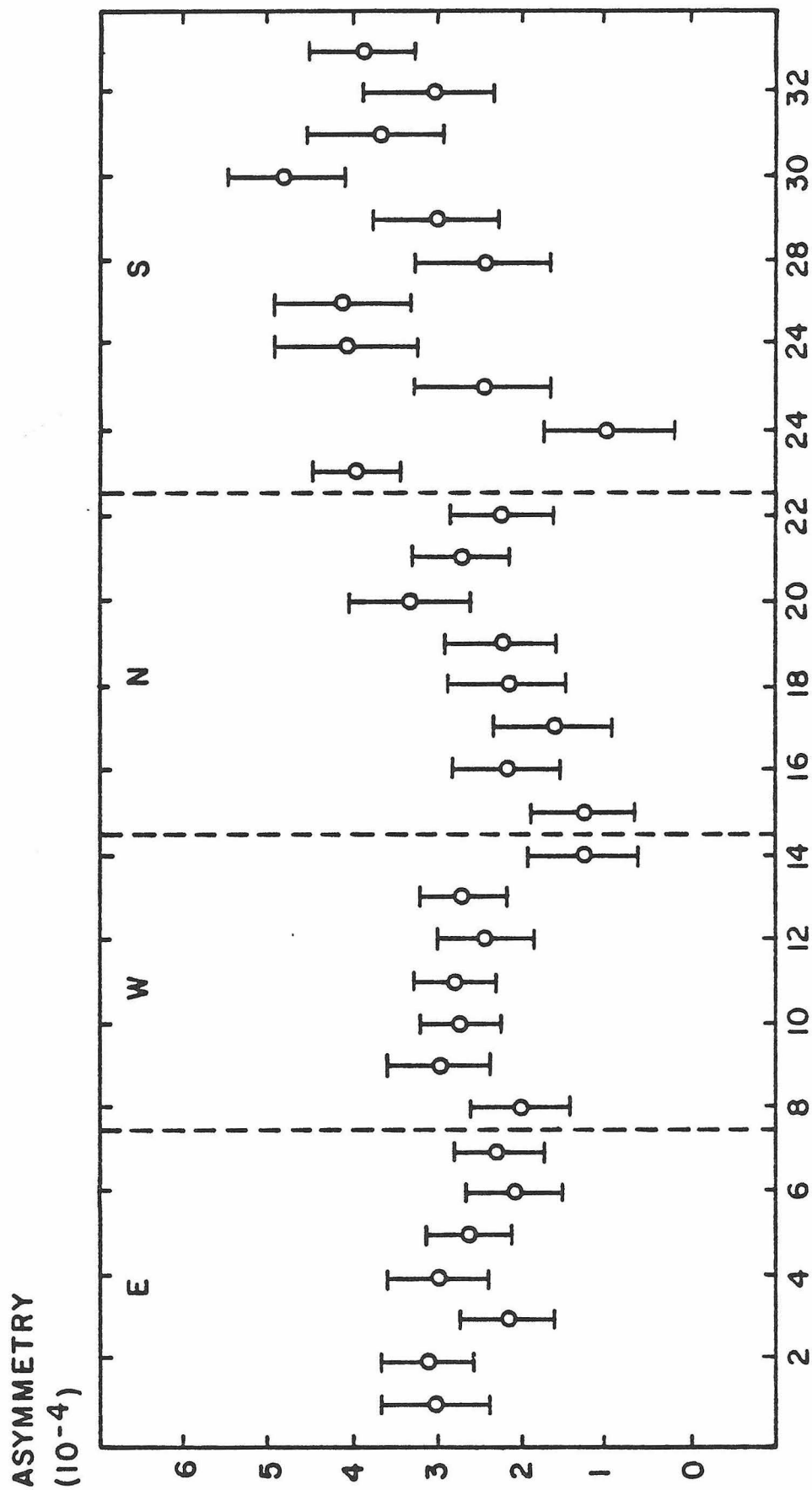

Fig. 11. Asymmetries of 33 runs of Experiment No. 1.

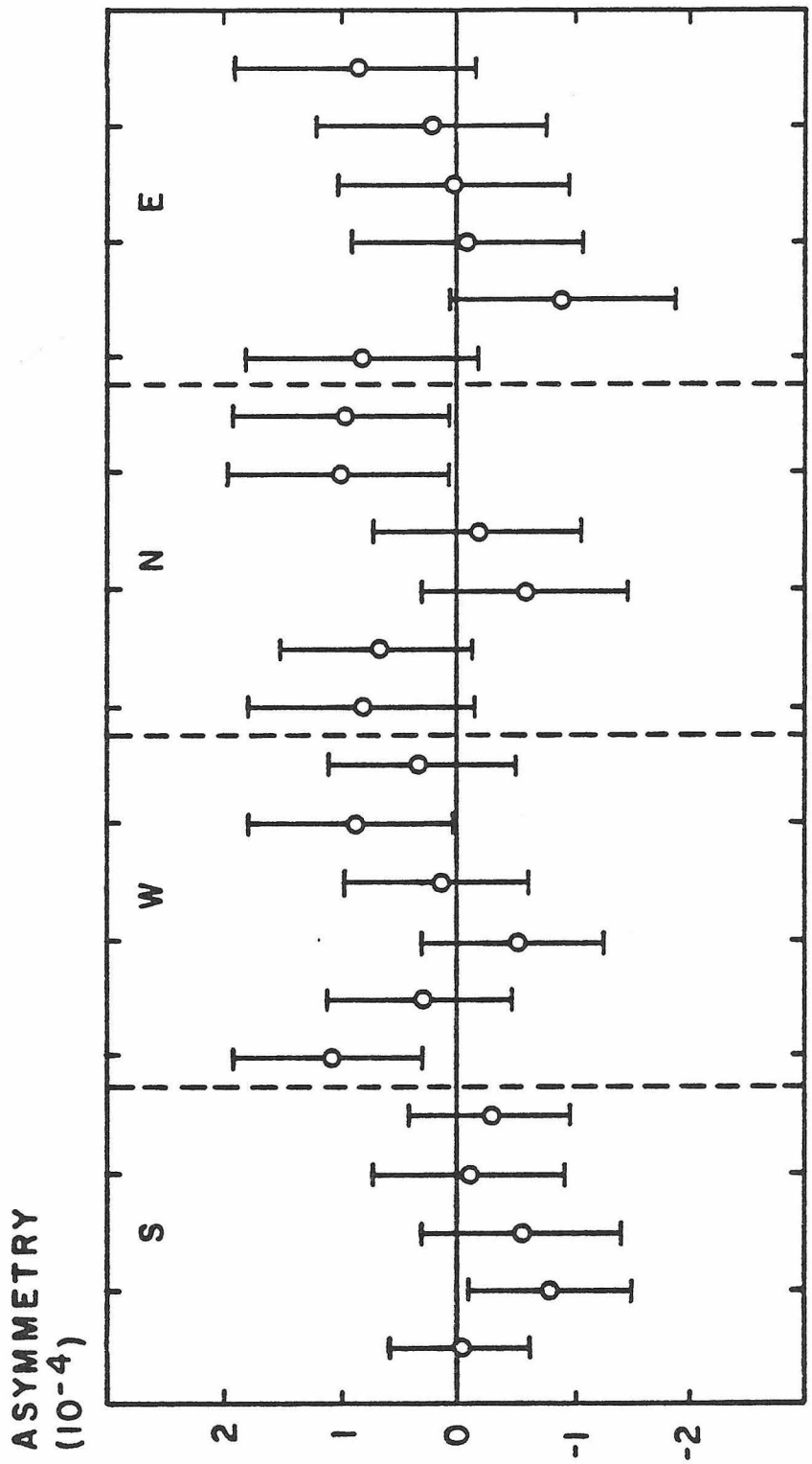

Fig. 12. Asymmetries of 23 control runs at 4K for Experiment No. 1.

with zero for these runs demonstrates the absence of significant instrumental effects not dependent upon polarization.

(ii) Improvements in experimental precision

The precision of the first experiment was limited by the large contribution of Ir x rays in the polarimeter spectrum. The previously discussed improvements in polarimeter shielding for the subsequent experiments resulted in a factor of two improvement in polarization efficiency, and hence a factor of two in increased sensitivity of our measurement to $\sin(\eta+\xi)$. Results for the first series of runs using the redesigned polarimeter (Experiment No. 2) are summarized in Table II. (The source for this experiment was a 0.018 mm ^{191}Os(Fe) foil, again indium-soldered to copper.) For this series of runs data were acquired consecutively in ψ and $\pi+\psi$ polarimeter positions (i.e. in NS and EW pairs) and averaged. (In later runs this procedure was found to be of crucial importance in the cancellation of residual field effects.) Data were also acquired for different cyclic permutations of the four NaI detectors located at ϕ = 45°, 135°, 225°, and 315°. Asymmetries for the 8 pairs of runs are tabulated, together with their corresponding source temperatures, effective polarizations, and background-to-signal coefficients. The reader may note the uniformly increasing values of f and $f_a B_3$ resulting from decreasing source strength and source heating as the ^{191}Os decays with 15.4 day half-life. From the weighted average over all pairs of runs a value $\sin(\eta+\xi) = (-4.97 \pm 0.30) \times 10^{-3}$ is obtained. Control runs at 4K yielded a null measurement $A' = (0.07 \pm 0.33) \times 10^{-4}$. The asymmetries A' for the 29 individual "cold" runs and 15 "warm" runs are respectively plotted in Fig. 13 and Fig. 14.

Table II. Results of Experiment No. 2.

Polarimeter Orientation	Temperature T(mK)	Polarization $f_a\langle B_3\rangle$	Background-to-Signal f	Raw Asymmetry $A'(10^{-4})$	Corrected Asymmetry $A\ (10^{-4})$	Phase $(\eta+\xi)$ (10^{-3})
NS (3)[a]	28.4	1.25(3)	0.06(3)	5.17(43)	5.48(46)	-4.90(41)
EW (3)	27.2	1.27	0.07	5.01(49)	5.36(52)	-4.72(46)
NS (2)	26.1	1.29	0.07	5.50(45)	5.88(48)	-5.10(42)
EW (2)	25.2	1.31	0.08	5.61(46)	6.06(50)	-5.17(43)
EW (4)	22.2	1.36	0.08	4.84(67)	5.23(72)	-4.30(59)
NS (4)	21.3	1.37	0.09	6.38(58)	6.95(63)	-5.67(51)
EW (2)	18.7	1.41	0.13	5.56(81)	6.28(92)	-4.97(73)
EW (4)	18.3	1.42	0.14	5.06(71)	5.77(81)	-4.53(64)
N(weighted average)	26	1.29	0.07	5.28(38)	5.65(41)	-4.90(36)
S	26	1.29	0.07	5.87(40)	6.28(43)	-5.44(37)
E	24	1.33	0.09	6.37(36)	6.94(39)	-5.83(33)
W	24	1.33	0.09	3.97(38)	4.33(41)	-3.64(34)
NS	26	1.29	0.07	5.56(28)	5.95(29)	-5.16(25)
EW	24	1.33	0.09	5.24(26)	5.71(28)	-4.79(24)
Weighted Average of NS,EW pairs	25	1.31(3)	0.08(3)	5.40(19)	5.83(26)[b]	-4.97(30)[c]
Control Runs						
N	4K	0.0		0.57(73)		
S				-0.27(60)		
E				0.78(71)		
W				-0.52(67)		
Weighted Average of N,S,E,W				0.07(33)		

Polarization efficiency = -0.435 ± 0.015.

χ^2_2 per 28 degrees of freedom = 1.6.
χ^2 per degree of freedom for NS,EW pairs = 0.64. Number of pairs = 8.

a) Data were acquired in pairs of ψ positions and for different ϕ polarimeter orientations; number in ( ) refers to the NaI counter at $\phi = 45°$.
b) Error includes (1 + f) uncertainty.
c) Includes errors of (1 + f), $f_a\langle B_3\rangle$, and E_p.

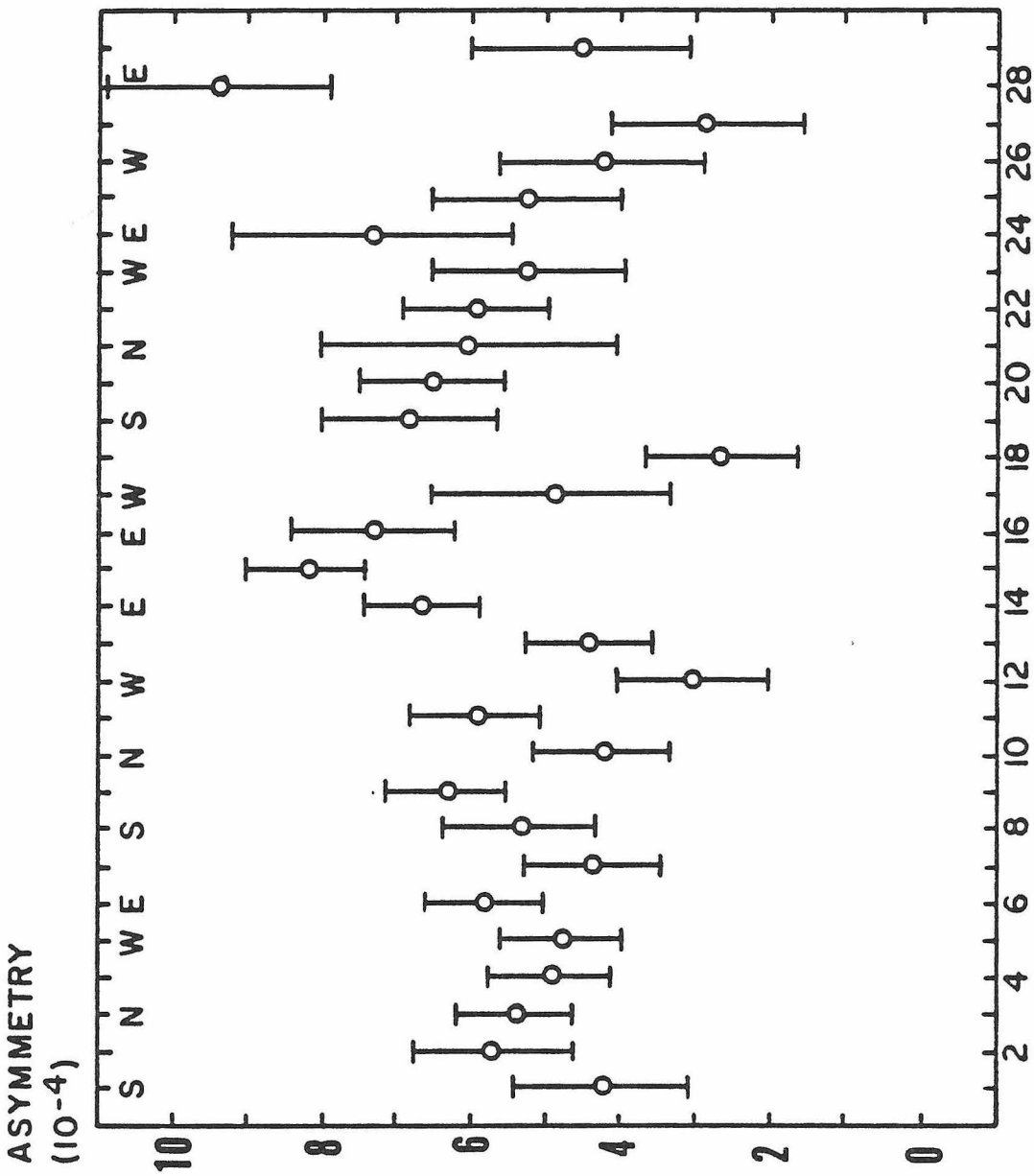

Fig. 13. Asymmetries of 29 runs of Experiment No. 2.

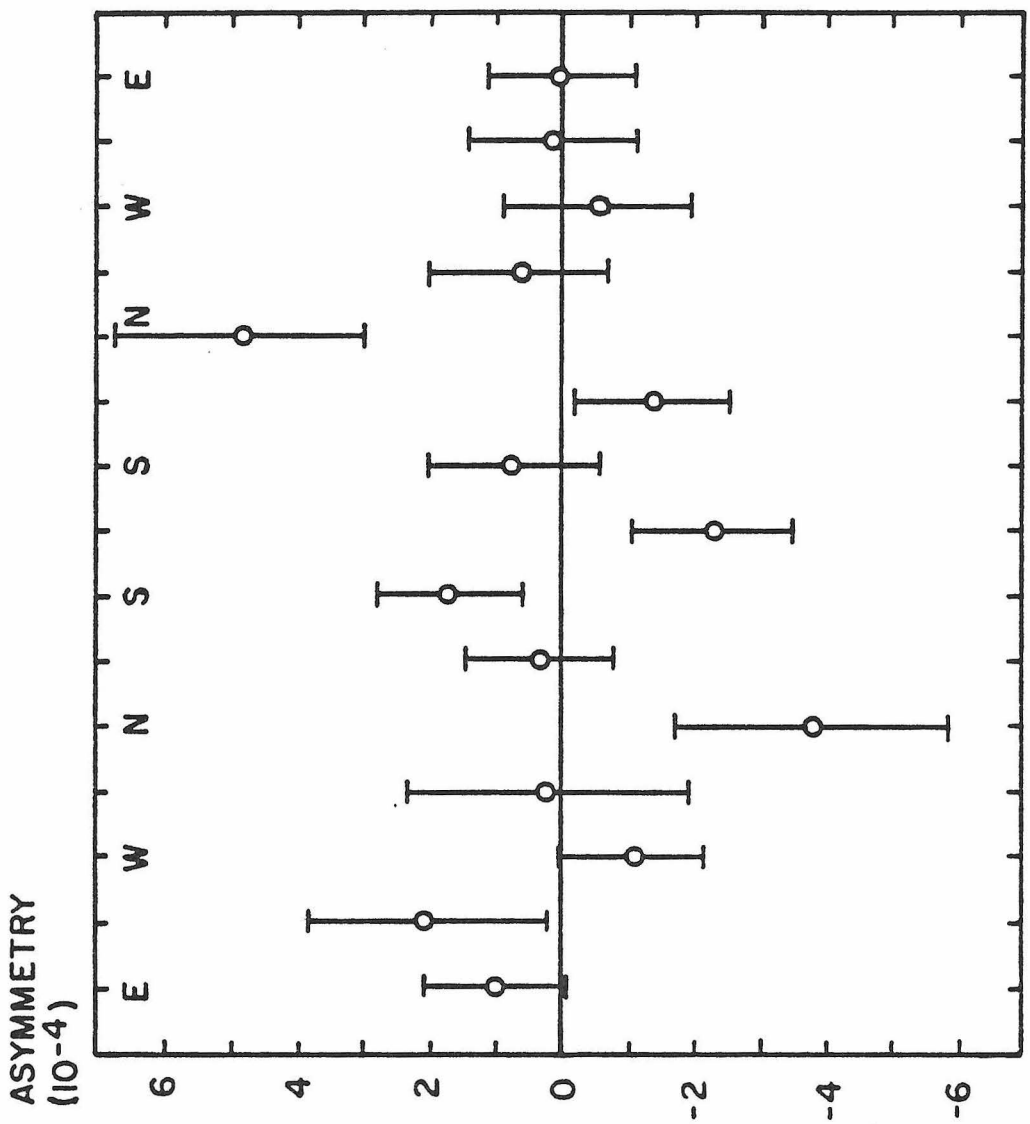

Fig. 14. Asymmetries of 15 control runs at 4K for Experiment No. 2.

(iii) Asymmetries due to residual fields

Table III and Table IV present the results for the final two experiments with ^{191}Ir. The source of Experiment No. 3 was a 0.02 mm thick Os(Fe) foil indium-soldered to platinum (Fig. 4b) to reduce the influence of magnetostrictive effects, (see discussion in Appendix B), while the fourth experiment reverted to a 0.025 mm thick foil soldered to copper. Data for the 20 and 22 runs of the two experiments were again acquired in NS and EW pairs and so tabulated. Respective weighted-average values $\sin(\eta+\xi) = (-4.94 \pm 0.40) \times 10^{-3}$ and $\sin(\eta+\xi) = (-4.48 \pm 0.34) \times 10^{-3}$ are obtained. ^{191}Ir-induced background was especially large for the fourth and final experiment. For this experiment the Sn ring of Fig. 5 was replaced by a similar Pb ring to reduce the background contribution.

Although NS and EW averaged data yield consistent results, the tabulated averages for individual N, S, E, and W positions reveal a significant divergence in results for opposing polarimeter orientations. (This is also evidenced in the large values of χ^2, which are reduced upon averaging N and S, and E and W measurements.) In particular, for both experiments asymmetries corresponding to south and east positions are higher than their north and west complements. This phenomenon also appears towards the end of Expt. 2 as evidenced in Fig. 13. Such an effect may be attributed to residual fields in the horizontal plane of the iron foil which result in a net orienting field vector that does not reverse by π along with the externally applied switching field. To account for the higher S and E asymmetries a residual field in the NE direction is required (see Appendix C). Although the earth's magnetic field should not be of sufficient magnitude at our level of precision to have any effect, its direction happens to correspond to these polarimeter

Table III. Results of Experiment No. 3.

Polarimeter Orientation	Temperature T(mK)	Polarization $f_a\langle B_3\rangle$	Background-to-Signal f	Raw Asymmetry $A'(10^{-4})$	Corrected Asymmetry $A\ (10^{-4})$	Phase $(\eta+\xi)$ (10^{-3})
EW (4)	33.4	1.14(3)	0.36(8)	3.85(31)	5.24(42)	-5.15(41)
NS (4)	32.3	1.17	0.39	3.38(41)	4.70(57)	-4.50(54)
NS (4)[a]	30.2	1.21	0.44	3.18(47)	4.58(68)	-4.24(63)
EW (4)[a]	29.3	1.22	0.46	3.43(50)	5.01(73)	-4.60(67)
NS (3)[a]	28.4	1.24	0.48	5.19(45)	7.68(67)	-6.93(60)
NS (3)	27.9	1.25	0.50	3.23(56)	4.84(84)	-4.33(75)
EW (3)[a]	26.9	1.27	0.53	3.74(47)	5.72(72)	-5.04(63)
EW (3)	25.8	1.29	0.54	3.98(56)	6.13(86)	-5.31(74)
NS (1)	25.3	1.30	0.56	2.64(60)	4.12(94)	-3.54(81)
EW (1)	24.8	1.30	0.58	3.50(60)	5.53(95)	-4.76(82)
N(weighted average)	29	1.22	0.45	3.00(30)	4.35(44)	-3.99(40)
S	29	1.22	0.45	4.26(31)	6.18(45)	-5.66(41)
E	30.5	1.20	0.45	4.67(29)	6.77(42)	-6.31(39)
W	30.5	1.20	0.45	2.96(27)	4.29(39)	-4.00(36)
NS	29	1.22	0.45	3.64(22)	5.29(32)	-4.86(29)
EW	30.5	1.21	0.45	3.74(20)	5.41(29)	-5.02(27)
Weighted Average of NS,EW pairs	30	1.21(3)	0.45(8)	3.69(15)	5.36(37)[b]	-4.94(40)[c]

Polarization efficiency $E_p = -0.435 \pm 0.015$.

χ^2 per 19 degrees of freedom = 2.4.
χ^2 per degree of freedom for NS,EW pairs = 1.9. Number of pairs = 10.

a) Earth-field compensated (see text).
b) Error includes (1 + f) uncertainty.
c) Includes errors of $f_a\langle B_3\rangle$, (1 + f), and E_p.

Table IV. Results of Experiment No. 4

Polarimeter Orientation	Temperature T(mK)	Polarization $f_a\langle B_3\rangle$	Background-to-signal f	Raw Asymmetry $A'(10^{-4})$	Corrected Asymmetry $A\ (10^{-4})$	Phase $(\eta+\xi)$ (10^{-3})	Ge Asymmetry $A_1(10^{-4})$	ϵ (10^{-3})
EW (2)	33.9	0.99(4)	0.15(5)	2.92(41)	3.36(47)	-3.81(53)		
EW (2)	32.2	1.02	0.17	3.18(37)	3.72(43)	-4.09(47)	21.8(8)	1.8
EW (2)[a]	31.0	1.05	0.18	3.12(34)	3.68(40)	-3.93(43)	3.2(5)	0.3
NS (2)[a]	29.8	1.05	0.20	3.20(35)	3.84(42)	-4.11(45)	6.9(5)	0.6
NS (2)	28.8	1.08	0.21	3.01(36)	3.64(44)	-3.78(46)	42.1(6)	3.5
NS (4) [b]	26.5	1.13	0.24	4.34(49)	5.38(61)	-5.34(60)	26.4(7)	2.2
NS (4)[a]	25.9	1.15	0.26	4.57(43)	5.76(54)	-5.61(53)	0.5(7)	0.0
EW (4)	25.2	1.19	0.27	4.62(55)	5.87(70)	-5.52(66)	33.7(9)	2.8
EW (4)[a]	24.8	1.20	0.28	3.79(47)	4.85(60)	-4.52(56)	14.7(10)	1.2
EW (4)	21.6	1.28	0.37	4.35(67)	5.96(92)	-5.21(80)	18.6(14)	1.5
EW (4)[a]	21.6	1.28	0.38	5.10(78)	7.04(1.08)	-6.15(94)	1.8(12)	0.1

(Continued)

Table IV. (continued)

	T(mK)	$f_a\langle B_3\rangle$	f	A'(10^{-4})	A (10^{-4})	$(\eta+\xi)$ (10^{-3})
N(Weighted[c] average)	29	1.09	0.22	2.21(42)	2.70(51)	-2.78(52)
S	29	1.09	0.22	4.67(41)	5.70(50)	-5.86(51)
E	30	1.04	0.18	4.09(34)	4.83(40)	-5.21(43)
W	30	1.04	0.18	2.97(32)	3.50(38)	-3.78(41)
NS	30	1.09	0.22	3.48(29)	4.24(36)	-4.36(36)
EW	31	1.04	0.18	3.49(23)	4.13(28)	-4.43(29)
NS,EW	30	1.06	0.20	3.48(18)	4.17(22)	-4.40(23)
N(Weighted[a] average)	30	1.08	0.22	3.78(39)	4.61(48)	-4.79(50)
S	30	1.08	0.22	3.71(38)	4.53(46)	-4.70(48)
E	29	1.10	0.21	3.25(38)	3.93(46)	-4.00(47)
W	29	1.10	0.21	3.82(36)	4.62(44)	-4.71(45)

(Continued)

Table IV. (continued).

	T(mK)	$f_a\langle B_3\rangle$	f	$A'(10^{-4})$	$A(10^{-4})$	$(\eta+\xi)$ (10^{-3})
NS[a]	30	1.08	0.22	3.74(26)	4.56(33)	-4.74(34)
EW	29	1.10	0.21	3.54(26)	4.30(32)	-4.38(32)
NS,EW	29	1.09	0.22	3.64(19)	4.43(23)	-4.55(23)
Weighted Average of All Runs	30	1.07(4)	0.21(5)	3.56(13)	4.29(24)[d]	-4.48(34)[e]

Polarization efficiency $E_p = -0.435 \pm 0.015$.

χ^2 per 21 degrees of freedom = 2.5.
χ^2 per 10 degrees of freedom for NS,EW pairs = 2.0.

a) Residual-field cancellation (see text).
b) For this and subsequent runs the source disk was rotated 90° about its axis relative to its original orientation.
c) Includes only those runs without residual-field cancellation.
d) Error includes uncertainty from (1 + f).
e) Error includes uncertainties from (1 + f), $f_a\langle B_3\rangle$, and E_p.

coordinates. To verify the negligibility of earth-field effects, an external coil wound about the outer shield of the refrigerator was used to cancel the vertical component of the earth's field, and the pair of superconducting coils orthogonal to the switching pair used to null that horizontal component. No discernable change occurred for the earth-field-compensated runs (these runs are so labeled in Table III), eliminating the earth's field as a source of systematic error.

More drastic measures were taken in the final experiment to investigate the effects of residual fields and to ascertain the effectiveness of the NS, EW averaging procedure. As shown in Appendix C, an imperfectly reversing field will result in an asymmetry A_1 in the intensity distribution $W_1(\theta)$ observed by the Ge detector given by

$$A_1 \simeq \frac{3Q_2B_2U_2A_2 \sin\theta \cos\theta \, \varepsilon}{1 + Q_2B_2U_2A_2P_2(\cos\theta)} , \tag{3.17}$$

where $\varepsilon = |H \text{ residual}|/|H \text{ applied}|$ and the reversing angle is $\pi - 2\varepsilon$. This asymmetry is zero at the normal detector location $\theta = 0^\circ$. During the fourth experiment the Ge detector was therefore located at $\theta = 45^\circ$ from the applied field (still in the horizontal plane of the source) to monitor ε. In this manner it was determined that residual fields corresponding to externally applied fields of a few gauss orthogonal to the 2-kG switching field were present in the Os(Fe) foil. Time-reversal measurements were then undertaken with and without a 4-G external field (maintained by the pair of coils orthogonal to the switching pair) to null the residual field. The data of Table IV reveal completely consistent EW and NS averaged results with and without residual-field cancellation, demonstrating the effectiveness of the

averaging procedure in cancelling the effects of residual fields. Table IV includes the Ge asymmetries A_1 together with their implied ε for each time-reversal run as illustration of the sensitivity of the A_1 measurement to the presence of residual fields and the effectiveness of the field cancellation for each run. From the averaged data for each of the four polarimeter orientations, it may be seen that the divergence between asymmetries of opposing orientations has disappeared for the field-nulled runs.

To determine if residual fields in the foil were endemic to the source itself, and perhaps related to source preparation, the source foil of Expt. 4 was rotated 90° clockwise about the vertical axis relative to its original orientation. This change was made about halfway through the experiment, as indicated in Table IV, and necessitated warming the refrigerator to room temperature. No residual fields were initially observed with the Ge detector upon recooling the source, but manifested themselves after a few days.

We now attribute the presence of the observed fields to imperfect demagnetization of the iron foil following temperature measurements. The technique for demagnetization involves the use of a logarithmically decreasing sinusoidal input to the superconducting coils. By observing the Ge asymmetry A_1 as a sensitive monitor of residual fields in the foil, demagnetization effectiveness could be investigated and optimized. The last few cycles of demagnetization are particularly important, as is the initial field strength. In particular it was determined that significant improvement in demagnetization could be obtained by increasing up to a factor of 2 the 500G starting field originally thought to be sufficient. This was used with success in the elimination of residual field effects in a later ^{131}Xe experiment (discussed in Sec. 4).

(iv) Final experimental results

Results for all four experiments are summarized in Table V. This table is a revised version of Table I of Ref. 20, which summarized the first three experiments. Significant changes are: (1) quoted polarization efficiencies $E_p = -0.23 \pm 0.02$ and $E_p = -0.43 \pm 0.03$ for the polarimeters are replaced by the revised efficiencies $E_p = -0.21 \pm 0.02$ and $E_p = -0.435 \pm 0.015$ which include background corrections for the polarimeter 1 result and the recent efficiency determination discussed in Sec. 3.6 using ^{57}Fe; and (2) background parameters $f = 0.07 \pm 0.03$ and $f = 0.37 \pm 0.08$ for Experiments 2 and 3 are replaced by $f = 0.08 \pm 0.03$ and 0.45 ± 0.08. Reflected in Table V are the slightly increased source strengths of the final two experiments which resulted in higher source temperatures and lower polarization coefficients. Because of ^{192}Ir contaminants these runs also display signficantly higher levels of background in the polarimeter spectrum, as indicated by the larger f values.

Consistent values of $\sin(\eta+\xi)$ are obtained for all experiments. From the weighted average of the four values a final result $\sin(\eta+\xi) = (-4.76 \pm 0.21) \times 10^{-3}$ is obtained. For subsequent discussions a value $\sin(\eta+\xi) = (-4.8 \pm 0.2) \times 10^{-3}$ will be adopted.

Table V. Final Results of the ^{191}Ir Experiments.

Experiment #	Temperature	Polarization		Polarization Efficiency	Background-to-Signal	Raw Asymmetry	Corrected Asymmetry	Phase ($\eta+\xi$)
	T(K)	$f_a\langle B_3\rangle$	$f_a\langle B_4\rangle$	E_p	f	$A'(10^{-4})$	$A\ (10^{-4})$	(10^{-3})
1)	0.024	1.35(3)	1.0	-0.21(2)	0.03(2)	2.52(11)	2.60(13)	-4.46(48)
(Control)	4.0	0.0	0.0			0.09(17)		
2)	0.025	1.31(3)	1.0	-0.435(15)	0.08(3)	5.40(19)	5.83(21)	-4.97(30)
(Control)	4.0	0.0	0.0			0.07(33)		
3)	0.030	1.21(3)	0.9	-0.435(15)	0.45(8)	3.69(15)	5.36(37)	-4.94(40)
4)	0.030	1.07(4)	0.7	-0.435(15)	0.21(5)	3.56(13)	4.29(24)	-4.48(34)
Weighted [a] Average of #s 2),3),4)								-4.83(23)
Weighted Average of All								-4.76(21)

a) Note that the same efficiency measurement E_p was used for Experiments 2)-4). Hence the uncertainty of $(\eta+\xi)$ is not the sum in quadrature of the uncertainties for each experiment.

CHAPTER 4

EXPERIMENT WITH ^{131}Xe

4.1 The Choice of Nuclear Transition

In order to obtain a direct measurement of the time-reversal phase η, it is necessary to select a transition where final state effects are negligible. We are thus restricted to low Z elements or high energy transitions. The requirement of a high degree of obtainable nuclear polarization - hence a large magnetic moment and hyperfine field - to some extent limits our direction toward lower Z elements. Simultaneously, shielding problems and lower polarization efficiency place some restriction on transition energy. The prominent 364 keV E2-M1 transition in ^{131}Xe was selected as a compromise between the various requirements. As shown in Fig. 15, the 364 keV level is directly populated from the β^- decay of ^{131}I. The oriented state is thus the parent ^{131}I, which has a magnetic moment μ = 2.738 ±0.001 μn[41], and a hyperfine field H = 1144.0 ±1.5 kG[42] for I(Fe) yields Δ = 32.7 mK. A mixing ratio δ = -4.53 ±0.12 (with $|\delta|/(1+|\delta|^2)$ = 0.21) is reported[43] for the 364 keV transition. With the substitution of appropriate spin coefficients, Eq. (2.1) becomes

$$W_{364}(\theta,\phi) = 1 + 0.205\ B_2P_2(\cos\theta) + 0.0390\ B_4P_4(\cos\theta)$$
$$+ E_p\left[-0.0130\ B_2P_2{}^2(\cos\theta) - 0.0326\ B_4P_4{}^2(\cos\theta)\right]\cos 2\phi$$
$$+ E_p\left[0.0292\ B_3P_3{}^2(\cos\theta)\right]\sin(\eta+\xi)\ \sin 2\phi. \qquad (4.1)$$

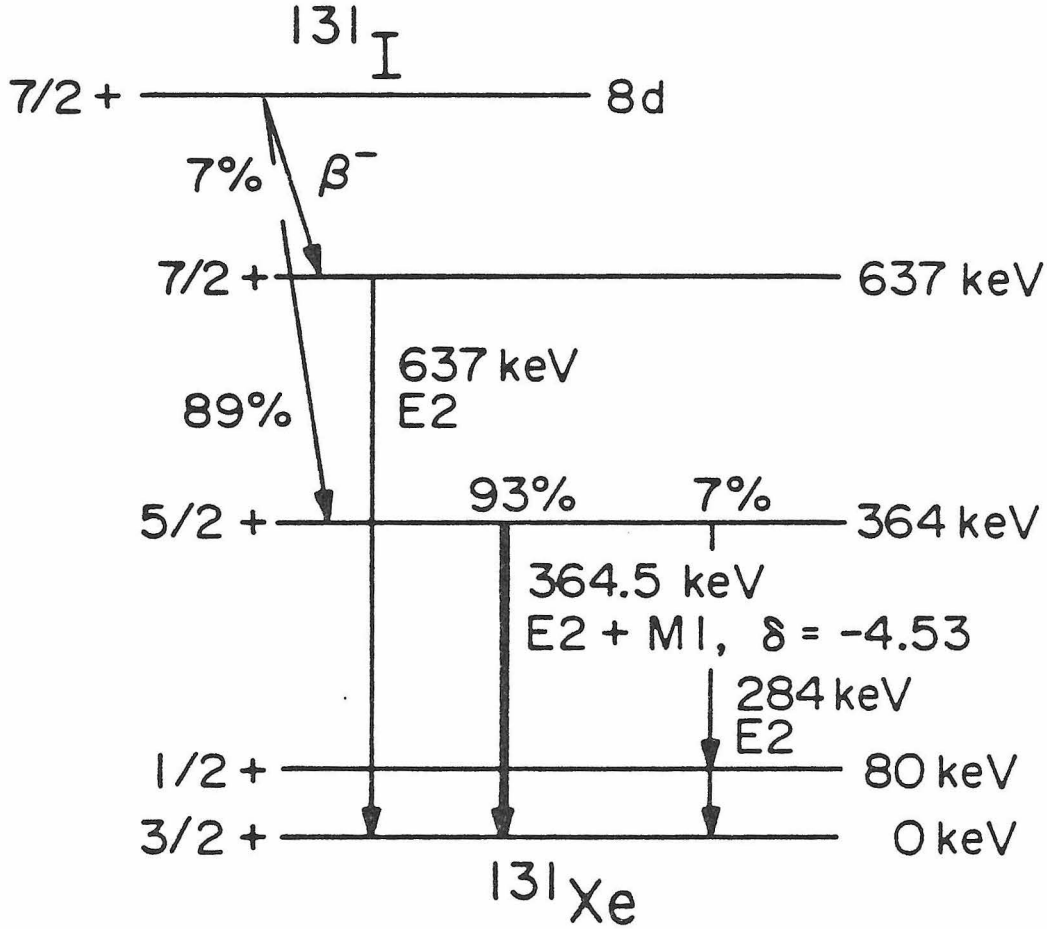

Fig. 15. Decay scheme of ^{131}I.

Since the 284 keV E2 transition (see Fig. 15) is unresolved from the 364 keV line in the scattered spectrum, the angular distribution $W_{284}(\theta,\phi)$ is included:

$$W_{284}(\theta,\phi) = 1 - 0.5345\ B_2P_2(\cos\theta) - 0.6172\ B_4P_4(\cos\theta) + E_p\left[-0.2338\ B_2P_2^{\,2}(\cos\theta) + 0.0298\ B_4P_4^{\,2}(\cos\theta)\right]\cos 2\phi. \quad (4.2)$$

4.2 Source Preparation

The ^{131}I(Fe) sources were prepared by the implantation of $^{131}I^{+}$ ions at 50 and 70 keV acceleration energies into 0.02 mm thick, 0.32 cm diameter iron foils (held at room temperature). The implantation was achieved at Argonne National Laboratory courtesy of Dr. J. Lerner. Prior to implantation the iron foils were polished, annealed in H_2 at 700 C, and indium-soldered to a copper collar button (Fig. 4c) at Caltech. The assembly was shipped to Argonne Labs in argon to minimize surface oxidation of the iron. Initial source activities of 0.5 to 1 mCi were obtained starting from 30 and 60 mCi samples of carrier-free ^{131}I purchased commercially from ICN[44] as NaI in 0.05 N NaOH solution. With a mean estimated penetration depth of 200 Å, the ^{131}I concentration in iron was less than 0.2 at.%.

Upon return the ^{131}I(Fe) foil, with activity ranging from 150 to 300 μCi, was cleaned with alcohol and freon to remove loose surface activity. The collar button assembly was then screwed into the cooling rod of the refrigerator and cooled to 30 mK.

4.3 Determination of Source Temperature and Nuclear Alignment

As in the case of ^{191}Ir, measurements with the Ge detector of the anisotropy in the intensity distribution $W_1(\theta)$ of oriented ^{131}Ir(Fe) indicated a degree of orientation systematically smaller than predicted by Eq. (2.2) at the estimated source temperature. This phenomenon is not unusual for ion implanted sources[45], and has been successfully explained in terms of low-field siting of some fraction of the ^{131}I[43],[46].

A procedure similar to that described in Sec. 3.4 was therefore adopted in determining an effective B_3. The fact that the ^{131}I activity lies within 200 Å of the foil surface, and the fear that any heating of the foil would change the siting, prohibited the soldering of a ^{60}Co(Fe) temperature-calibration source to the ^{131}I(Fe) after an experiment. For two initial ^{131}I sources, temperature was estimated to within a few mK from the known source activity (source heating) and from a temperature-calibrated carbon resistor fixed to the mixing chamber of the refrigerator. A more accurate calibration was made for a third source with a ^{60}Co(Fe) foil indium-soldered to a 0.32 cm slotted, threaded copper stud which was tightened down onto the collar button assembly with a copper nut (Fig. 4d). For this third source a two-parameter fit of the observed ^{131}I anisotropy $W_1'(0)/W_1'(90)$ to the ^{60}Co-determined temperature, with

$$W_1'(\theta) = 1 + 0.204\, f_a B_2(f_s \Delta/T) P_2(\cos\theta) + 0.379\, f_a B_4(f_s \Delta/T) P_4(\cos\theta) \quad (4.3)$$

for the 364 keV transition, yielded a high-field-siting fraction f_a = 0.49 ±0.02 and a saturation parameter f_s = 0.90 ±0.03.

The latter parameter corresponds to an effective hyperfine field of 1030 kG, somewhat lower than the NMR-measured field of 1144 kG. Mossbauer studies on ^{131}I(Fe) sources indicate the existence of intermediate-field sites[46],[47], so our effective measured field may correspond to a combination of sites at both fields.

For the less accurately calibrated initial sources the parameter f_s was held fixed at $f_s = 0.90$. Fits for f_a yielded $f_a = 0.23 \pm 0.01$ and $f_a = 0.48 \pm 0.01$ respectively for the first and second sources. The much lower alignment observed for the first source was attributed to an inadequate implanation energy of 50 keV, for which a large proportion of the ^{131}I was believed to reside in the surface oxidation layer of the iron foil. A larger implanation energy of 70 keV for the two following sources yielded the consistently larger values of $f_a \simeq 0.49$. As in the case of ^{191}Ir, orientation coefficients $B_k(\Delta/T)$ were replaced by effective coefficients $f_a B_k(f_s \Delta/T)$ throughout.

4.4 Modification of the Polarimeter and Determination of Polarization Efficiency E_p

(i) Revised Shielding

The Sn collimating ring and plate depicted in Fig. 5 proved to be inadequate for shielding the NaI counters from the direct 364 keV gamma ray of ^{131}Xe. They were therefore replaced by an analogous Pb ring and plate. This effectively halved the background. The background-to-signal ratio, determined from a comparison of NaI spectra with and without the Al scattering block in place (see Fig. A.2), was nevertheless large, with $f = 1.5 \pm 0.3$. The NaI energy spectrum, with SCA window settings, is shown in Fig. 16.

(ii) Deterimination of E_p by Monte Carlo calculation

Because of the large background and the poor alignment of ^{131}I, an accurate determination of polarization efficiency at 364 keV via measurement of A_p' proved unfeasible. In light of its fair success at 129 keV, a Monte Carlo calculation yielding $E_p = -0.41 \pm 0.01$ for the Compton polarimeter was taken as the efficiency at 364 keV. The quoted "error" is the standard deviation of n runs divided by $\sqrt{n}$. To reflect the uncertainty in the calculation's reproduction of real polarimeter-source geometry, a polarization efficiency $E_p = -0.41 \pm 0.03$ was adopted.

(iii) Experimental corroboration of the Monte Carlo determination

Measurements of A_p' were carried out at $\theta = 90^\circ$ and 54.7° despite the above-mentioned difficulties. Taking an intensity ratio of 93:7 between the

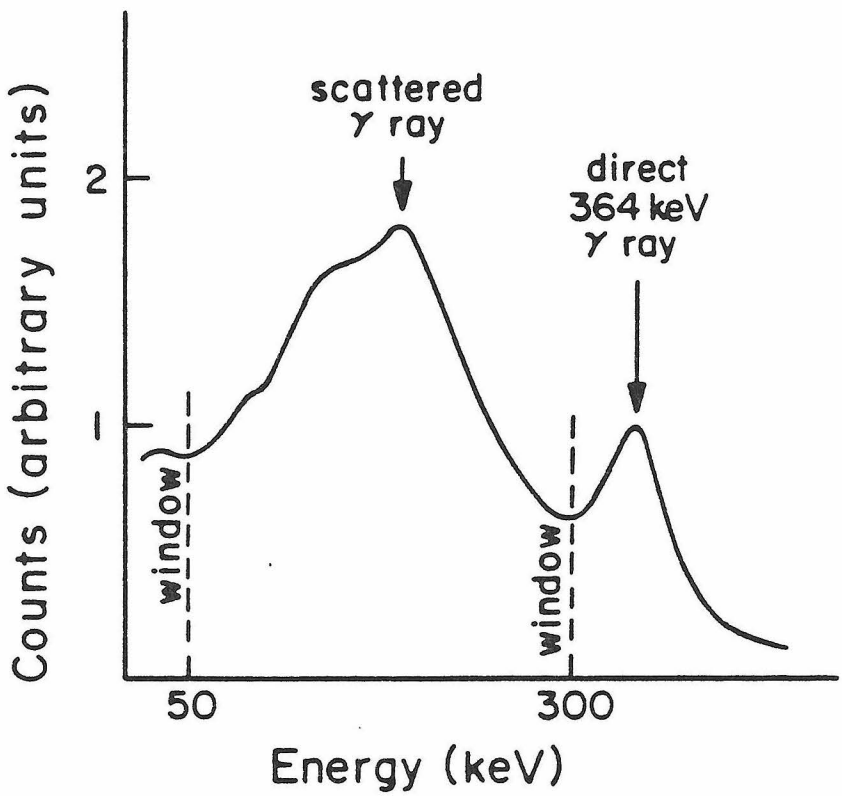

Fig. 16. NaI spectrum for ^{131}Xe.

(unresolved) 364 and 284 keV lines, and assuming nearly equal polarization efficiencies for both lines, combining (4.1), (4.2), and (3.4) yields a polarization asymmetry

$$A_p(\theta) = \frac{W(\theta,\ \phi = 0^\circ) - W(\theta,\ \phi = 90^\circ)}{W(\theta,\ \phi = 0^\circ) + W(\theta,\ \phi = 90^\circ)}$$

$$= E_p \frac{-0.137\ Q_2 f_a B_2 P_2{}^2(\cos\theta) - 0.0282\ Q_4 f_a B_4 P_4{}^2(\cos\theta)}{1 + 0.158\ Q_2 f_a B_2 P_2(\cos\theta) + 0.338\ Q_4 f_a B_4 P_4(\cos\theta)} . \quad (4.4)$$

Solid angle corrections Q_k for the polarimeter and effective orientation coefficients $f_a B_k$ have been included. At $\theta = 90^\circ$ and 54.7° this becomes

$$A_p(90) = E_p \frac{-0.405\ f_a B_2 + 0.199\ f_a B_4}{1 - 0.0777\ f_a B_2 + 0.119\ f_a B_4} , \quad (4.5)$$

$$A_p(54.7) = E_p \frac{-0.270\ f_a B_2 + 0.177\ f_a B_4}{1 - 0.124\ f_a B_2} . \quad (4.6)$$

Measurements of A_p' were carried out with and without the Al scattering block. As discussed in Appendix A, the measured asymmetry A_p' is a linear combination of the asymmetry A_p of the scattered 364 keV line and the background asymmetry A_B;

$$A_p' = (A_p + A_B f)/(1 + f). \quad (4.7)$$

Solving for A_p gives

$$A_p = A_p'(1 + f) - A_B f. \quad (4.8)$$

Taking A_B to be the asymmetry measurement without scatterer, the 90° measurements at 25 mK yielded $A_p' = 0.0310$ and $A_B = 0.0024$, from which $A_p = 0.074$ is determined. From (4.5), with $f_a B_2 = 0.51$ and $f_a B_4 = 0.12$, we obtain $E_p = -0.40$.

Similarly, 54.7° measurements gave $A_p' = 0.0197$ and $A_B = -0.0084$, from which a background-corrected asymmetry $A_p = 0.062$ is deduced, yielding $E_p = -0.39$. Both measurements are fortuitously consistent with the adopted value $E_p = -0.41 \pm 0.03$.

4.5 Results

Three measurements with three ^{131}I sources have been performed. Data were acquired as in the ^{191}Ir experiments in NS and EW polarimeter orientation pairs.

(i) Results for the first two experiments

For the first preliminary experiment a 50 keV implantation energy was utilized in the preparation of the ^{131}I(Fe) source. An initial ion source activity of 30 mCi yielded an activity of about 150 μCi upon cooldown. Results for this run are summarized in Table VI. The effect of residual fields is clearly illustrated in the averaged data for N, S, E, and W positions, with opposing polarimeter orientations producing nearly equal asymmetries of opposite sign. To determine an average raw asymmetry A', unweighted averages for each pair of runs were taken, with an assigned error equal to the largest statistical uncertainty of the two runs divided by $\sqrt{2}$. A weighted average over all pairs then yielded $A' = (2.2 \pm 1.9) \times 10^{-5}$, and a background-corrected value $A = (5.4 \pm 4.8) \times 10^{-5}$. Assuming 93% intensity of the 364 keV line, and with spin coefficients R = -0.1387 and S = 0.4093, one may determine $\sin(\eta+\xi)$ via (3.15):

$$\sin(\eta+\xi) = A \frac{1 - 0.143\, f_a B_4}{(0.151 \pm 0.004)\, f_a B_3 E_p} \quad . \tag{4.9}$$

With $f_a B_3 = -0.15 \pm 0.02$ [in contrast to Ir(Fe), I(Fe) has a positive hyperfine field; Δ is therefore positive and B_3 negative[35]], $f_a B_4 = 0.06$, and $E_p = -0.41 \pm 0.03$, we obtain $\sin(\eta+\xi) = (5.8 \pm 5.3) \times 10^{-3}$. Table VI includes the result of a control experiment at 4K, for which $A' = (1.2 \pm 2.6) \times 10^{-5}$.

Table VI. Results of ^{131}Xe Experiment No. 1.

Polarimeter Orientation	Temperature T(mK)	Polarization $f_a\langle B_3\rangle$	Raw Asymmetry $A'(10^{-5})$	Corrected Asymmetry $A\ (10^{-5})$	Phase $(\eta+\xi)$ (10^{-3})
NS(3) [a]	22.5	-0.145(20)	5.45(2.91)	13.62(7.28)	15.04(8.04)
EW(3)	22.5	-0.145	0.58(3.51)	1.45(8.78)	1.60(9.69)
NS(3)	22	-0.150	-1.45(4.91)	-3.62(12.28)	-3.86(13.11)
EW(3)	22	-0.150	-0.56(4.94)	-1.40(12.35)	-1.49(13.18)
N(weighted average)	22	-0.147	23.90(3.49)	59.75(8.72)	65.07(9.49)
S	22	-0.147	-16.80(3.21)	-42.00(8.02)	-45.74(8.76)
E	22	-0.146	-7.17(3.97)	-17.92(9.92)	-19.65(10.88)
W	22	-0.146	7.50(3.72)	18.75(9.30)	20.56(10.20)
NS	22	-0.147	3.66(2.50)	9.14(6.26)	9.87(6.85)
EW	22	-0.146	0.20(2.86)	0.49(7.15)	0.52(7.81)
Weighted Average of NS,EW pairs	22	-0.147(20)	2.16(1.88)	5.39(4.75) [b]	5.80(5.27) [c]
Control Runs					
N	4K	0.0	14.00(5.05)		
S			-3.20(5.27)		
E			-1.19(4.78)		
W			-6.06(5.51)		
Weighted Average of N,S,E,W			1.20(2.56)		

Polarization efficiency $E_p = -0.41 \pm 0.03$.

Background-to-signal $f = 1.5 \pm 0.03$.

χ^2 per degree of freedom for NS,EW pairs = 0.8. Number of pairs = 4.

a) Asymmetries for $\psi, \pi+\psi$ pairs are unweighted averages of the two orientations.
b) Error includes uncertainty from $(1 + f)$.
c) Includes errors from $(1 + f)$, $f_a\langle B_3\rangle$, and E_p.

Implantation energy was increased to 70 keV for a second source, with the result of improved siting for the I(Fe). With double the initial ion activity, a usable source activity of 300 μCi was achieved. Data are presented in Table VII. Improved statistics gave $A' = (-1.0 \pm 1.0) \times 10^{-5}$ and $A = (-2.6 \pm 2.5) \times 10^{-5}$. As in the first experiment, unweighted averages of pairs of ψ and $\pi + \psi$ polarimeter orientations were taken to cancel residual field effects. With the improved polarization $f_a B_3 = -0.24 \pm 0.03$ at 28mK, $\sin(\eta+\xi)$ was determined to be $(-1.5 \pm 1.7) \times 10^{-3}$. [The reader may note that the averaged $\langle \sin(\eta+\xi) \rangle \propto \langle A/B_3 \rangle \neq \langle A \rangle / \langle B_3 \rangle$ in this case.]

(ii) Results for Experiment No. 3

Table VIII summarizes the results of a third ^{131}Xe measurement which used a source similar to that of Expt. 2. Asymmetries for the 12 runs, each of approximately 24 h duration, are plotted in Fig. 17. In comparison with the initial experiment, the more recent series of runs are characterized by an absence of nonzero, opposite-signed asymmetries for opposing ψ orientations. This is attributed to the improved demagnetization technique developed during the fourth ^{191}Ir experiment (discussed in (iii) of Sec. 3.8). [In time-ordered sequence, the first two ^{131}Xe experiments occurred prior to the final ^{191}Ir run, while the third ^{131}Xe experiment occurred subsequently.] From the raw asymmetry $A' = (-0.9 \pm 0.8) \times 10^{-5}$, a background-corrected asymmetry $A = (-2.3 \pm 2.1) \times 10^{-5}$ is obtained. The phase $(\eta + \xi)$ was determined from the weighted average of NS and EW pairs to be $\sin(\eta+\xi) = (-1.5 \pm 1.5) \times 10^{-3}$. Control runs at 4K were also performed, with the null result $A' = (-0.7 \pm 1.0) \times 10^{-5}$.

Table VII. Results of ^{131}Xe Experiment No. 2.

Polarimeter Orientation	Temperature T(mK)	Polarization $f_a\langle B_3\rangle$	Raw Asymmetry $A'(10^{-5})$	Corrected Asymmetry $A\ (10^{-5})$	Phase $(\eta+\xi)$ (10^{-3})
NS (1) [a]	31	-0.200(30)	-4.59(1.82)	-11.48(4.55)	-9.16(3.63)
EW (1)	30	-0.215	0.93(1.63)	2.32(4.08)	1.72(3.03)
NS (1)	25	-0.280	-0.12(1.69)	-0.30(4.22)	-0.17(2.40)
N(weighted average)	27	-0.25	33.91(1.58)	84.72(3.95)	54.10(2.52)
S	28	-0.24	-39.28(1.46)	-98.20(3.65)	-65.28(2.43)
E	30	-0.22	-22.50(2.33)	-56.25(5.82)	-40.79(4.22)
W	30	-0.21	23.84(2.10)	59.60(5.25)	45.28(3.99)
NS	27	-0.247	-2.19(1.24)	-5.47(3.09)	-2.90(2.00)
EW	30	-0.215	0.93(1.63)	2.32(4.08)	1.72(3.03)
Weighted Average of NS,EW pairs	28	-0.236(30)	-1.05(0.99)	-2.63(2.48) [b]	-1.50(1.69) [c]
Control Runs					
N	4K	0.0	0.76(2.58)		
S			-3.22(3.23)		
E			3.17(2.96)		
W			0.11(2.32)		
Weighted Average of N,S,E,W			0.34(1.35)		

Polarization efficiency $E_p = -0.41 \pm 0.03$.

Background-to-signal $f = 1.5 \pm 0.3$.

χ^2 per degree of freedom for NS,EW pairs = 2.9.

a) Asymmetries for NS,EW pairs are unweighted averages of the two orientations.
b) Error includes uncertainty from (1 + f).
c) Error includes uncertainties from (1 + f), $f_a\langle B_3\rangle$, and E_p.

Table VIII. Results of ^{131}Xe Experiment No. 3.

Polarimeter Orientation	Temperature T(mK)	Polarization $f_a\langle B_3\rangle$	Raw Asymmetry $A'(10^{-5})$	Corrected Asymmetry $A\ (10^{-5})$	Phase $(\eta+\xi)$ (10^{-3})
NS (3)	32	-0.196(30)	-2.01(1.80)	-5.02(4.50)	-4.09(3.67)
EW (3)	31	-0.204	-0.57(1.74)	-1.42(4.35)	-1.11(3.40)
NS (3)	30	-0.217	-1.54(1.88)	-3.85(4.70)	-2.83(3.46)
EW (3)	29	-0.233	0.87(1.92)	2.18(4.80)	1.49(3.29)
NS (3)	27	-0.250	-5.68(2.91)	-14.20(7.28)	-9.07(4.65)
EW (3)	26	-0.265	2.35(2.59)	5.88(6.48)	3.54(3.90)
N(weighted average)	30.5	-0.214	-4.07(1.68)	-10.12(4.20)	-7.96(3.13)
S	30.5	-0.214	-0.81(1.68)	-2.02(4.20)	-1.43(3.13)
E	29	-0.232	0.30(1.64)	0.75(4.10)	0.75(2.81)
W	30	-0.223	0.76(1.63)	1.90(4.08)	1.52(2.91)
NS	30.5	-0.214	-2.43(1.19)	-6.08(2.97)	-4.70(2.21)
EW	29	-0.227	0.53(1.15)	1.33(2.88)	1.12(2.02)
Weighted Average of NS,EW pairs	30	-0.221(30)	-0.90(0.83)	-2.26(2.09)[a]	-1.53(1.52)[b]
Control Runs					
N	4K	0.0	1.38(2.18)		
S			0.19(1.98)		
E			-2.16(1.95)		
W			-1.93(2.20)		
Weighted Average of N,S,E,W			-0.67(1.03)		

Polarization efficiency $E_p = -0.41 \pm 0.03$.

Background-to signal $f = 1.5 \pm 0.3$.

χ^2 per 11 degrees of freedom = 1.1.
χ^2 per degree of freedom for NS,EW pairs = 1.2.

a) Error includes uncertainty from $(1 + f)$.
b) Includes uncertainties from $(1 + f)$, $f_a\langle B_3\rangle$, and E_p.

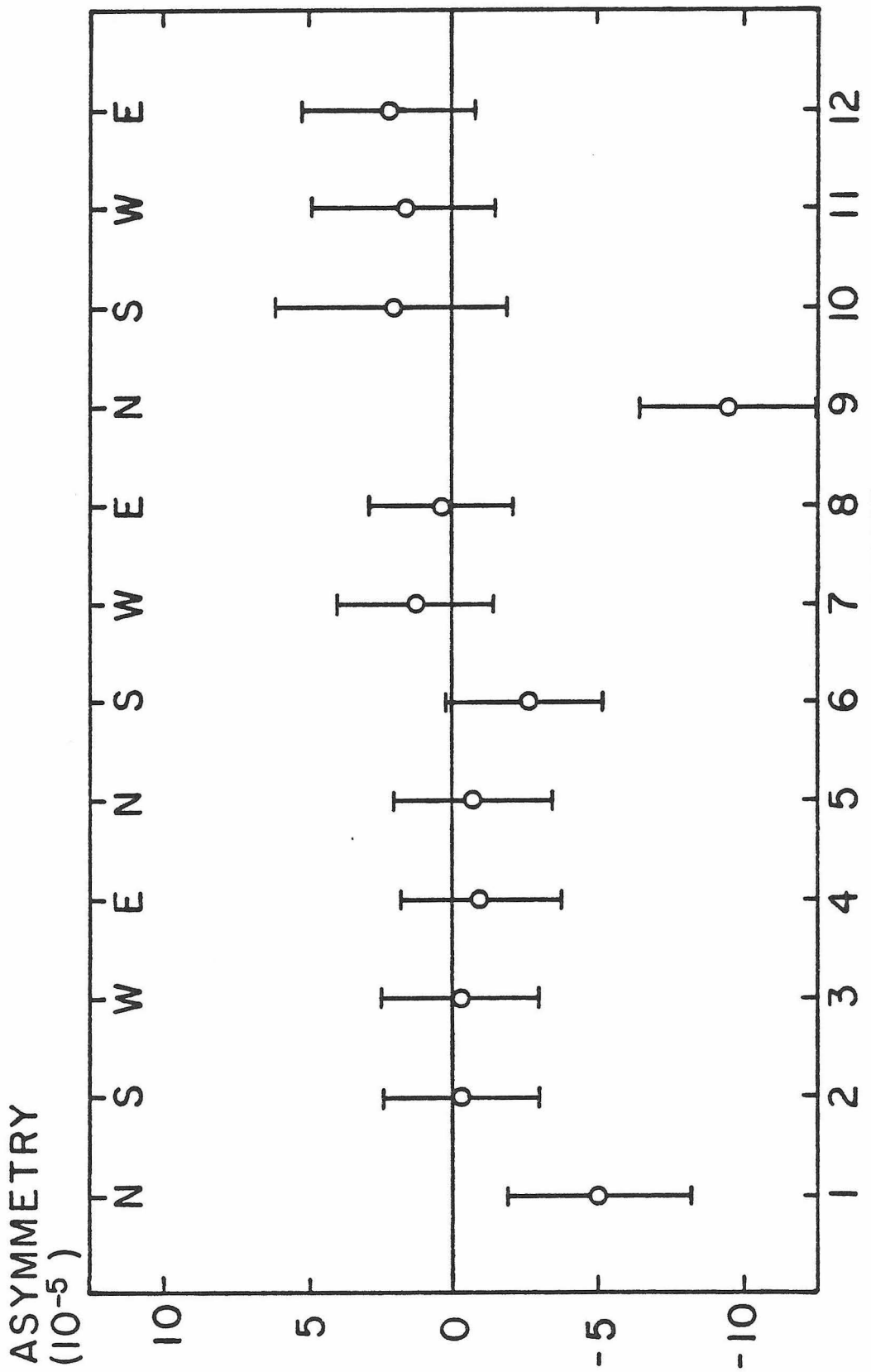

Fig. 17. Asymmetries for 12 runs of ^{131}Xe Experiment No. 3.

(iii) Final results

Final results for the three ^{131}Xe experiments are summarized in Table IX. The same polarization efficiency $E_p = -0.41 \pm 0.03$ and background-to-signal $f = 1.5 \pm 0.3$ have been adopted for all three experiments. A weighted average of the three measurements yields $\sin(\eta+\xi) = (-1.2 \pm 1.1) \times 10^{-3}$.

Table IX. Summary of ^{131}Xe Experiments.

Experiment #	Temperature	Polarization		Raw Asymmetry	Corrected Asymmetry	Phase ($\eta+\xi$)
	T(mK)	$f_a\langle B_3\rangle$	$f_a\langle B_4\rangle$	$A'(10^{-5})$	$A\ (10^{-5})$	(10^{-3})
1)	0.022	-0.15(2)	0.06	2.2(1.9)	5.4(4.8)	5.8(5.3)
(Control)	4.0	0.0	0.0	1.2(2.6)		
2)	0.028	-0.24(3)	0.09	-1.0(1.0)	-2.6(2.5)	-1.5(1.7)
(Control)	4.0			0.3(1.4)		
3)	0.030	-0.22(3)	0.08	-0.9(0.8)	-2.3(2.1)	-1.5(1.5)
(Control)	4.0			-0.7(1.0)		
Weighted Average						-1.2(1.1)

Polarization efficiency $E_p = -0.41 \pm 0.03$.

Background-to-signal $f = 1.5 \pm 0.3$.

CHAPTER 5

DISCUSSION

5.1 Atomic Final State Interaction in ^{191}Ir

The present observation of a nonvanishing value of $\sin(\eta+\xi) \simeq (\eta+\xi) = -(4.8 \pm 0.2) \times 10^{-3}$ for the mixed 129 keV γ transition in ^{191}Ir may be explained in terms of atomic final state effects. In Ref. 20 a comparison of the experimental result with the available calculated final state phases of Goldwire and Hannon[26] was made. From their work we found a "virtual-internal-conversion" phase shift $\xi_C = \xi_C(E2) - \xi_C(M1) = -4.51 \times 10^{-3}$ and a "virtual-Thomson-scattering" phase shift $\xi_R = \xi_R(E2) - \xi_R(M1) = 0.80 \times 10^{-3}$ between the two multipole components of the 129 keV transition. The total phase shift for the two final state processes was $\xi = \xi_C + \xi_R = -3.7 \times 10^{-3}$, with a quoted error of a few percent. Although of the same sign and order of magnitude, the calculated phase ξ differed from the measured $(\eta+\xi)$ by some five standard deviations. If it was assumed that no time-reversal violation (TRV) of this magnitude was present, the experimental observation could not be reconciled with the calculated atomic final state phase shift. [Contributions from other known TRV-simulating processes of "Faraday rotation" (see discussion in Ref. 19) and nuclear final state effects[22] are estimated to be $<10^{-6}$ and negligible at the present level of precision.]

The discrepancy between calculation and measurement, apparent evidence for a time-reversal violation, has motivated the recent theoretical study of atomic final state effects by Davis et al.[23]. Their calculations for ^{191}Ir yield for the conversion phase shift ξ_C for the atomic K, L, M, and N shell electrons, respectively, -3.85×10^{-3}, -0.97×10^{-3}, -0.23×10^{-3}, and

-0.05×10^{-3}, giving a total of $\xi_C = -5.10 \times 10^{-3}$. The phase shift for Rayleigh scattering (including Thomson scattering and the small "anomalous" scattering term) is $\xi_R = 0.79 \times 10^{-3}$. The total atomic final state phase shift then becomes $\xi = \xi_C + \xi_R = (-4.3 \pm 0.4) \times 10^{-3}$ (the indicated error bars represent a 2% uncertainty for the E2 and M1 phases). Our measured value is in agreement with the given upper limit of -4.7×10^{-3}. The revised calculations thus remove the apparent evidence for violation of time reversal invariance.

In summary, by measuring the linear polarization of the mixed 129 keV γ ray in ^{191}Ir oriented in iron, we have established for the first time a non-vanishing T-odd angular correlation in a nuclear transition. The reduced matrix-element ratio for the two competing multipoles (M1 and E2) was found to have an imaginary component with a phase angle of $(-4.8 \pm 0.2) \times 10^{-3}$. This time-reversal-like phase shift may be attributed to virtual quantum electrodynamical effects in the atomic final state, and is now accounted for by the final state calculations of Davis et al.[23]. The precision of the measurement is half an order of magnitude greater than all previous time-reversal measurements in low energy nuclear physics. By comparison with the theoretical bounds $-3.9 \times 10^{-3} \leq \xi \leq -4.7 \times 10^{-3}$ given by Davis, a limit $-10^{-3} \leq \eta \leq 0$ may be inferred, consistent with time reversal invariance.

5.2 General Survey; Experimental Evidence for Final State Effects

Experimental evidence for atomic final state effects in nuclear transitions is obtained primarily from Mossbauer experiments. Such experiments are sensitive to a dispersion term in the absorption cross section proportional to ξ_D, with

$$\xi_D = [\xi(M1) + |\delta|^2\xi(E2)]/(1 + |\delta|^2),$$

rather than the direct phase shift $\xi = \xi(E2) - \xi(M1)$. Table X lists the results of atomic final state phase measurements for various transitions together with the calculated phases of Davis[23]. Agreement between experiment and theory is in general quite good. Included is the result of a Mossbauer experiment which also measured the 129 keV transition in ^{191}Ir; a value $\xi_D = (-0.50 \pm 0.12) \times 10^{-3}$ is to be compared to the theoretically calculated $\xi_D = -0.69 \times 10^{-3}$. The measurement ξ_D is sensitive to a combination of M1 and E2 phases nearly orthogonal to the TRV-simulating phase ξ, however, so no comparison can be made with the present observation. We note that with the exception of the present ^{191}Ir measurement, the listed time-reversal measurements of the phase $\xi = \xi(E2) - \xi(M1)$ are all essentially null results.

Table X. Survey of Atomic Final State Measurements from Mossbauer and Correlation Experiments[23]

Isotope	E(keV)	Multipolarity	100ξ[a]	$100\xi_{EXPT.}$[b]
$^{57}_{26}Fe$	122.1	M1 + 1.4%E2	$\xi = -0.06$[c]	$\xi = -0.03 \pm 0.07$
$^{73}_{32}Ge$	13.3	E2	-3.24	-4.7 ± 1.0
$^{99}_{44}Ru$	90.0	E2 + 37%M1	-0.60	-0.33 ± 0.32
			$\xi = -0.57$[c]	$\xi = -0.43 \pm 0.50$
$^{131}_{54}Xe$	364.5	E2 + 4.6%M1	$\xi = -0.01$[c]	$\xi = -0.12 \pm 0.11$[d]
$^{153}_{63}Eu$	97.4	E1	-2.03	-1.1 ± 0.3 -1.4 ± 0.3
$^{155}_{64}Gd$	86.5	E1	-2.48	-2.5 ± 0.5
	105.3	E1	-1.85	-1.8 ± 0.5
$^{161}_{66}Dy$	25.6	E1	-3.97	-3.5 ± 0.5 -3.2 ± 0.3
	74.5	E1	-3.40	-3.0 ± 0.5
$^{166}_{68}Er$	80.6	E2	-1.37	-1.60 ± 0.19
$^{170}_{70}Yb$	84.3	E2	-1.33	-1.70 ± 0.38
$^{171}_{70}Yb$	66.7	M1 + 49%E2	-0.75	-1.00 ± 0.14
$^{180}_{72}Hf$	93.3	E2	-1.27	-1.82 ± 0.48
$^{181}_{73}Ta$	6.21	E1	-12.3	$-11. \pm 1.$
$^{182}_{74}W$	100.1	E2	-1.22	-1.71 ± 0.14
$^{183}_{74}W$	99.1	E2	-1.22	-1.25 ± 0.17
	46.5	M1 + 0.6%E2	-0.28	-0.05 ± 0.06

(continued)

Table X.(continued).

Isotope	E(keV)	Multipolarity	100ξ [a]	$100\xi_{EXPT.}$ [b]
$^{184}_{74}W$	111.1	E2	-1.17	-1.53 ± 0.29
$^{186}_{74}W$	122.5	E2	-1.10	-2.09 ± 0.36
$^{186}_{76}Os$	137.2	E2	-1.02	-1.02 ± 0.25
$^{188}_{76}Os$	155.0	E2	-0.93	-1.51 ± 0.49
$^{191}_{77}Ir$	129.5	M1 + 14%E2	-0.69	-0.50 ± 0.12
			ξ = -0.43 [c]	ξ = -0.48 ± 0.02 [d]
$^{193}_{77}Ir$	73.1	M1 + 31%E2	ξ = -0.12 [c]	ξ = 0.11 ± 0.38 ξ = 0.16 ± 0.24
$^{195}_{78}Pt$	98.7	M1	-0.70	-1.1 ± 0.3
$^{197}_{79}Au$	77.3	M1 + 12.1%E2	-0.40	-0.414 ± 0.017
$^{236}_{92}U$	45.3	E2	+0.31	+0.25 ± 0.75
$^{237}_{93}Np$	59.6	E1	-3.18	-3.4 ± 0.2

a) Calculated interference parameters ξ of Davis[23]. Both conversion and scattering contributions included.
b) Measured values of ξ.
c) For Time-Reversal Violation Experiments, $\xi = \xi(E2) - \xi(M1)$.
d) Present work.

5.3 Limit for Time Reversal Invariance in ^{131}Xe

A phase angle $\sin\eta = (-1.2 \pm 1.1) \times 10^{-3}$ was measured for the mixed (E2, M1) transition of 364 keV in ^{131}Xe. [At this energy, the atomic final state phase ξ is estimated by Davis[23] to be $\simeq -1 \times 10^{-4}$, and may be neglected.] The precision of the measurement is comparable to the best limits in literature [$\sin\eta = (-0.3 \pm 0.7) \times 10^{-3}$[19], $\sin\eta = (1.0 \pm 1.7) \times 10^{-3}$[15], $\sin\eta = (1.5 \pm 2.2) \times 10^{-3}$[48]], and is consistent with time-reversal invariance. One should note that the sensitivity of given experiment to a T-violating interaction depends on presently unknown matrix elements. Possible enhancement of TRV matrix elements could increase this sensitivity by orders of magnitude[9]. Theoretical estimates are therefore required to fully realize the implications of a particular experiment. In the meantime it seems justified to measure more than one case with the greatest possible precision.

High precision was obtained in the ^{131}Xe and ^{191}Ir measurements primarily because they are single counting experiments in contrast with the older coincident measurements. However, one must measure the relatively insensitive $k = 3$ term instead of the $k = 1$ term in the angular distribution. To achieve high precision requires a nearly ideal combination of large spin coefficients (U_3 and F_3) and a high degree of nuclear orientation (large magnetic moment and hyperfine field, and low temperature). In addition the poor energy resolution of the linear polarimeter limits the technique to cases where the γ-ray spectrum is simple. Common to all time-reversal experiments measuring nuclear γ transitions are the requirements of a large degree of multipole mixing ($\delta \simeq 1$) and small atomic final state interactions which simulate time reversal violation (thereby restricting one to high energy

transitions and/or low Z nulcei). In the case of ^{131}Xe, a factor of maybe 1.5 improvement in precision could be obtained by sacrificing some polarimeter solid angle for improved shielding from the direct γ ray to reduce background. Present generation dilution refrigerators, available commercially, for example from S.H.E.[49], are able to cool to 10 mK with fairly large source heat loads. A factor of 2 in increased nuclear orientation could be achieved in ^{131}Xe if temperatures of 10 to 15 mK could be reached. It seems doubtful, however, that a sensitivity for sinη approaching 10^{-4} or better for time-reversal tests in nuclei could be achieved with any currently available experimental techniques.

5.4 General Survey of Time-Reversal Measurements in Gamma Decay

A survey of time reversal measurements in nuclear γ decay is presented in Table XI. All measurements are consistent with time reversal invariance, and with the most recent limit for the neutron dipole moment $d_n < 1.6 \times 10^{-24}$ e cm[7]. One must note that the observables measured in the neutron dipole moment case are P-odd and T-odd, in contrast to the case of γ decay, for which P-even, T-odd observables are measured. A comparison between theory and experiment requires more accurate estimates than are presently available for the expected effect of a given theory on various T-odd observables.

The neutron dipole moment limit tends to rule out millistrong, electromagnetic, and possibly milliweak theories of time reversal violation, and is more easily reconciled with the superweak theories. However, precise interpretation of this limit, as in the case of γ decays, is difficult at present. If a superweak theory of T violation is correct, it would be impossible to measure a violation of time reversal invariance in nuclear γ transitions.

Table XI. Survey of Time-Reversal Experiments [19].

Isotope	Method[a]	Cascade (keV)	δ[b]	$10^3 x \sin\eta$
^{36}Cl	n-γ-γ	7790-790	0.21	4 ± 12
^{36}Cl	n-γ-γ	7790-790	0.21	-1.8 ± 2.2
^{49}Ti	n-γ-γ	341-1378	0.1	17 ± 25
^{56}Fe	β-γ-γ	2110-847	0.18	4 ± 26
^{56}Fe	β-γ-γ	1811-847	-0.28	
^{57}Fe	J-γ-ε	122	0.12	-0.31 ± 0.65
^{99}Ru	M.E.	90	-1.65	1.0 ± 1.7
^{106}Pd	β-γ-γ	1050-512	0.21	30 ± 40
^{106}Pd	β-γ-γ	1050-512	0.21	4 ± 18
^{110}Cd	J-γ-γ	1505-658	-1.09	1.5 ± 2.2
^{110}Cd	J-γ-γ	1384-658	-0.39	-1.7 ± 5.1
^{131}Xe[c]	J-γ-ε	364	-4.53	-1.2 ± 1.1
^{169}Tm	J-γ-γ	198-110	-0.30	150 ± 120
^{169}Tm	J-γ-γ	177-130	-0.51	≥ 0
^{175}Lu	J-γ-γ	283-114	-0.036	170 ± 500
^{180}Hf	J-γ-γ	501-332&215	5.3	48 ± 87
^{191}Ir[c]	J-γ-ε	129	0.40	$\lvert\eta\rvert < 10^{-3}$
^{193}Ir	M.E.	73	0.56	1.1 ± 3.8
^{193}Ir	M.E.	73	0.56	1.6 ± 2.4
^{192}Pt	J-γ-γ	604-316	-2.1	4 ± 5

a) M.E. stands for Mossbauer effect.
b) All mixing is E2-M1 except in ^{175}Lu(E1-M1) and ^{180}Hf(E3-M2).
c) Present work.

APPENDIX A

CORRECTIONS FOR BACKGROUND

Background in the polarimeter spectrum dilutes the measured time-reversal asymmetry (no background asymmetry was observed in an analysis of the background portion of the time-reversal polarimeter spectra), so that

$$A' = A[S/(S + B)]$$

$$= A/(1 + f), \qquad (A.1)$$

where A' is the measured asymmetry and A is the "true" asymmetry of the Compton-scattered "signal." The parameter $f \equiv B/S$ is defined as the ratio of background (B) to signal (S). To determine f for the ^{191}Ir experiments, energy spectra were acquired with the collimating window of the polarimeter shielding "blacked out" with a 2mm Pb absorber to effectively remove the scattered signal. A comparison of spectra with and without the Pb asorber is shown in Fig. A.1. Counts below and above the dashed curve are taken to be background (B) and signal (S) events, respectively. In this manner mean values of f = 0.03 ±0.02, 0.08 ±0.03, 0.45 ±0.08, and 0.21 ±0.05 were determined for experiments 1, 2, 3, and 4, respectively. The large background for the final two experiments was due to ^{192}Ir contaminants in the source. Because of the different half-lives of ^{191}Ir and ^{192}Ir, f is time dependent.

For the ^{131}Xe experiments, a background spectrum was obtained by removing the aluminum scatterer. From a comparison of the two spectra of Fig. A.2, a value f = 1.5 ±0.3 was deduced.

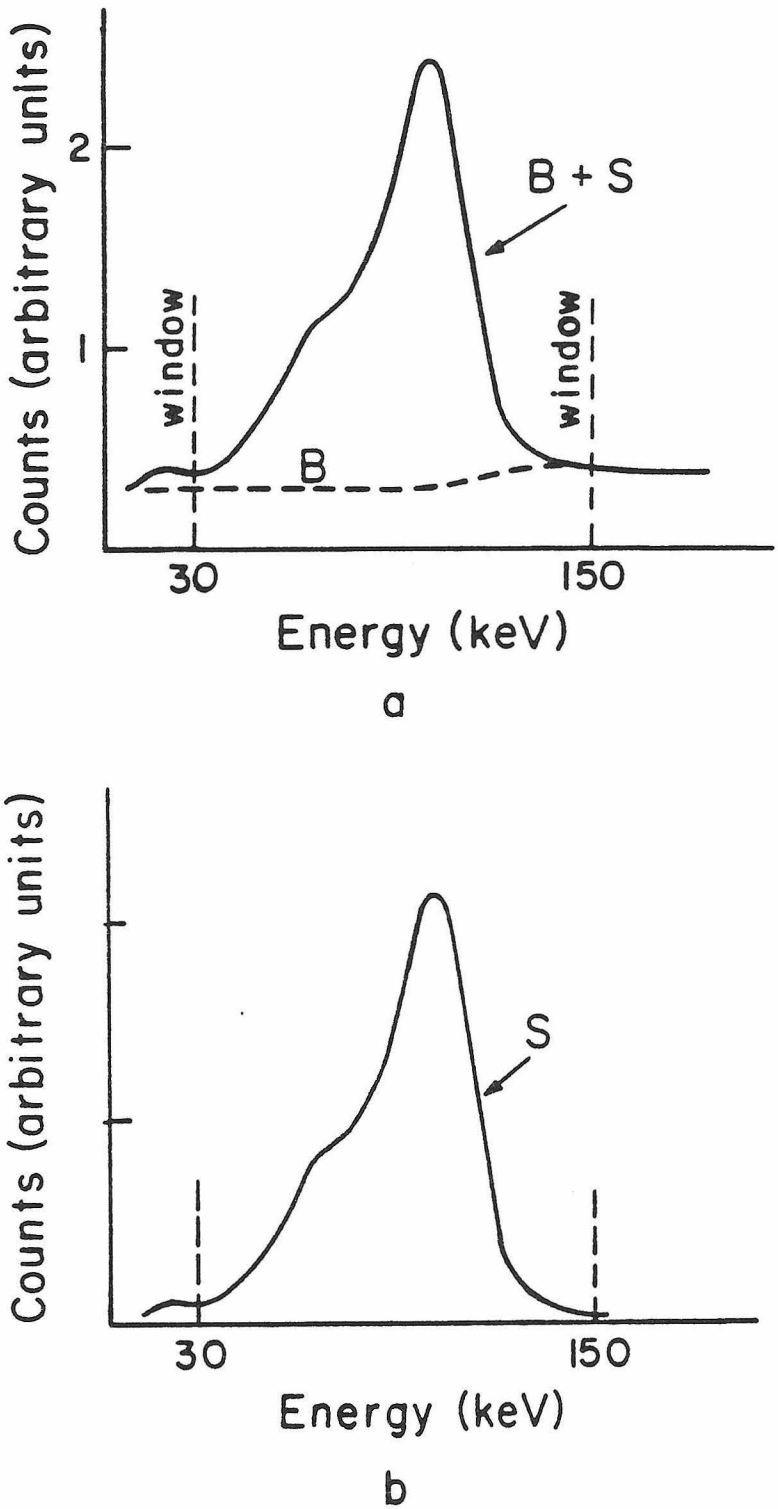

Fig. A.1. Background-subtraction spectra for ^{191}Ir. Entire photopeak, including background (B) and signal (S) is shown in (a). Background-subtracted spectrum is shown in (b).

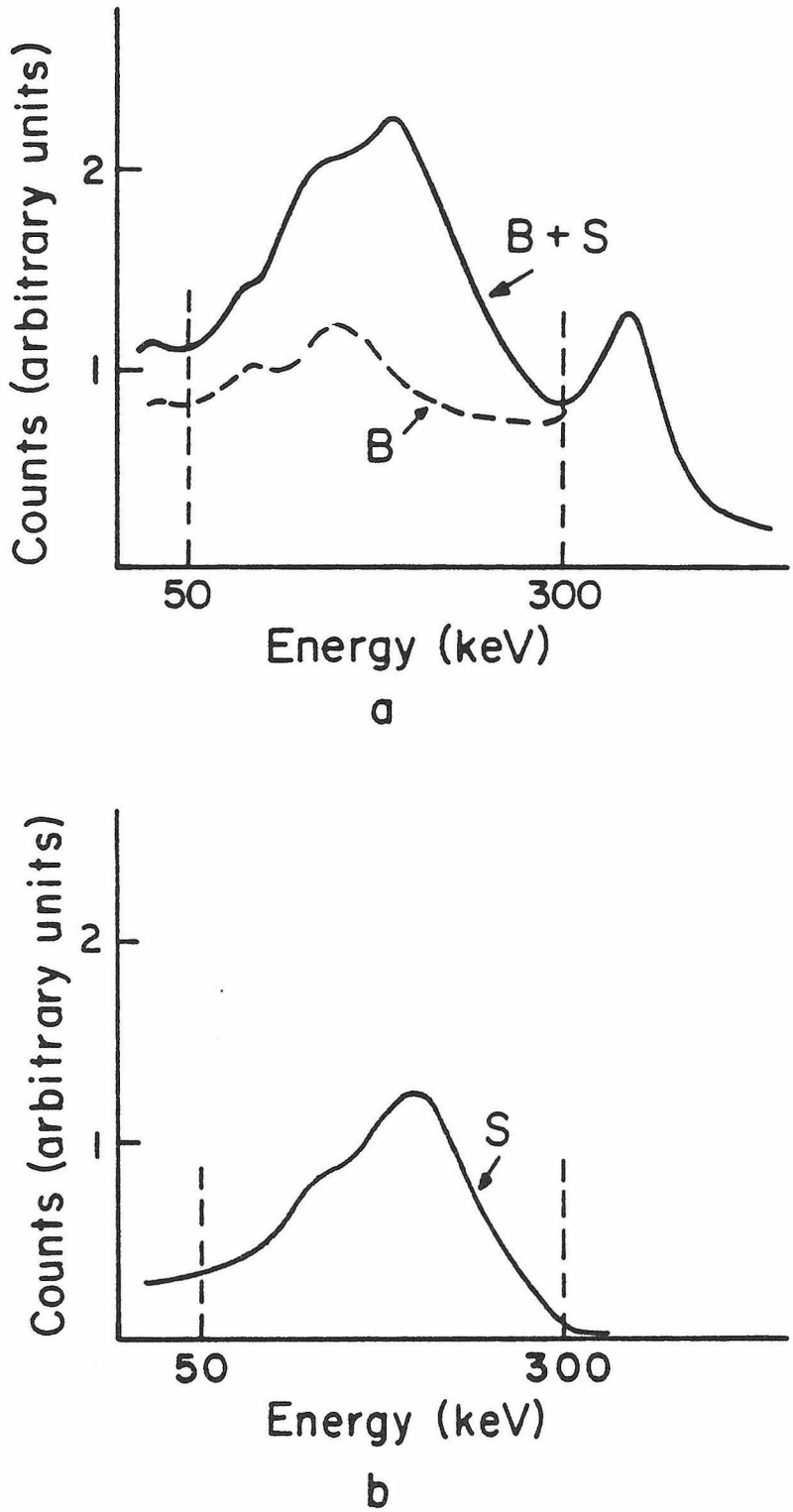

Fig. A.2. Background-subtraction spectra for ^{131}Xe. Entire photopeak, including background (B) and signal (S) is shown in (a). Background-subtracted spectrum is shown in (b).

The presence of background in the spectrum can cause biased polarization efficiency measurements in the following manner. The efficiency E_p of the polarimeter is determined (see Sec. 3.6) by measuring the asymmetry

$$A_p'(\theta) = \frac{W'(\theta,\phi=0^\circ) + W'(\theta,180^\circ) - W'(\theta,90^\circ) - W'(\theta,270^\circ)}{W'(\theta,0^\circ) + W'(\theta,180^\circ) + W'(\theta,90^\circ) + W'(\theta,270^\circ)} \qquad (A.2)$$

for $\theta = 54.7^\circ$ and 90°, where $W' = B + S$ is the total count rate in the window of Fig. A.1. However, background due to direct radiation from the source will also exhibit an asymmetry

$$A_B = \frac{B(\theta_0) + B(\theta_{180}) - B(\theta_{90}) - B(\theta_{270})}{B(\theta_0) + B(\theta_{180}) + B(\theta_{90}) + B(\theta_{270})}, \qquad (A.3)$$

where the angles θ_ϕ are the angles between the applied field and the directions defined by a line from source to NaI counters corresponding to (θ,ϕ). The background for the (θ,ϕ) detector is

$$B(\theta_\phi) = W(\theta_\phi)\, B_{4K}(\theta_\phi), \qquad (A.4)$$

with $W(\theta)$ the directional distribution of Eq. (2.1), and $B_{4K}(\theta)$ the background count rate at T = 4K. [The $B_{4K}(\theta_\phi)$ are deduced by measuring A_p' at 4K temperature. $B_{4K}(\theta)$ is not isotropic because of the anisotropic absorption of the superconducting coils (the reader is referred to Fig. 5).] The measured asymmetry A_p' is a linear combination of the "true" asymmetry A_p of the Compton-scattered signal and the background asymmetry A_B;

$$\begin{aligned} A_p' &= A_p[S/(S+B)] + A_B[B/(S+B)] \\ &= (A_p + A_B f)/(1+f). \end{aligned} \qquad (A.5)$$

Solving for A_p gives

$$A_p = A'_p(1+f) - A_B f. \tag{A.6}$$

For the ^{191}Ir experiments, direct radiation from both ^{191}Ir and ^{192}Ir contributes to background. As the asymmetry A_B for the two contributions is different, Eq. A.6 becomes

$$A_p = A'_p(1+f) - A_{B1} f_1 - A_{B2} f_2, \tag{A.7}$$

where the two contributions are identified by the subscripts 1 and 2, and $f_1 = B1/S$, $f_2 = B2/S$. The relative amounts of the two background contributions may be roughly determined by investigating the time behavior of the background. The sensitivy of the correction $\sum A_{Bi} f_i$ to the relative amounts of background radiation, however, severely limits the accuracy of the efficiency measurement if significant source-related background is present.

APPENDIX B

INVESTIGATION OF THE EFFECTS OF MAGNETOSTRICTION

During the investigation of the saturation and alignment characteristics of ^{191}Ir(Fe) it was observed that after demagnetizing both horizontal components of field in the source foil the Ir nuclei exhibited an anomalous orientation in the vertical direction (perpendicular to the foil plane) as if a field of several kG along that direction was present in the iron. This "field" remained unaffected by demagnetization along the vertical axis, however, and later measurements with a gaussmeter indicated that no vertical field existed! By comparing the 129 keV emission rates to the isotropic rates at 4K with the Ge detector, a directional distribution pattern for the zero-applied-field condition was mapped and found to assume the form of (3.3) if one empirically inserts another factor h in front of the polarization coefficients, i.e.

$$W(\theta) = 1 + h\, f_a B_2 U_2 A_2 P_2(\cos\theta), \qquad (B.1)$$

where now θ is the angle measured from the vertical axis, and h = 0.42. (The small P_4 term has been omitted.) This at first puzzling vertical orientation is now attributed to magnetostrictive effects caused by the differential contraction of iron and copper at low temperatures. Thermal expansion coefficients for iron and copper are 12×10^{-6} and 16.6×10^{-6} K^{-1} respectively; the iron, contracting less than the copper, therefore experiences a net radial compression force upon cooling. The factor h may then be interpreted as an effective normalized $\langle P_2(\cos\theta)\rangle$ which is nonzero because of the magnetostrictively-induced alignment of domains orthogonal to the foil plane.

Fortunately, the vertical domain alignment is apparently not associated with a macroscopic field of specified direction. Such a vertical field would be recognizable as producing an asymmetry in total polarimeter count rate during the time reversal runs (see Appendix C), although it should not affect the measured value of A' because the individual asymmetries of the four detectors are averaged with alternating sign (Eq. (3.13)). In fact all indications are that the magnetostrictively induced alignment is completely (although only temporarily) erased when the foil is saturated by an external field. However, to test the hypothesis of magnetostriction as a possible cause for the incomplete polarization observed for Ir(Fe), and to further examine any unforseen influences of magnetostriction on our measurements, a new source collar button was designed consisting of a 0.33 cm long, 0.25 cm diameter platinum rod surrounded by a 0.25 mm thick copper sleeve (Fig. 4b). [The copper sleeve was found to be necessary to maintain sufficiently high thermal conduction at mK temperatures.] Platinum's thermal expansion coefficient (9×10^{-6} K^{-1}) is closer to iron than is that of copper, and is actually smaller, so that upon cooling the Os(Fe) foil, indium-soldered to the platinum collar button, experiences a net radial expansion. Measurement of the directional distribution of this new source under the condition of zero applied field revealed a radial alignment (or absence of vertically oriented domains, as predicted for a foil under expansion) equivalent to $h = -0.13$ in Eq. (3.14). Calibration of this source polarization with ^{60}Co, however, yielded identical values of the parameters f_a and f_s as for the previous copper-mounted source which experienced a much larger and opposite magnetostrictive tendency. Also, no significant change in the time-reversal runs was observed, thereby reassuring us as to the negligibility of the effects of magnetostriction on our measurements.

APPENDIX C

ASYMMETRIES CAUSED BY AN IMPERFECTLY REVERSING FIELD

C.1 Effect of a Vertical Field

Let us consider a fixed vertical component of field H_v present in the source foil in addition to the horizontal field H induced by the external switching field. The net aligning field is then $\vec{H}_{\pm} = \pm\vec{H} + \vec{H}_v$ which as shown in Fig. C.1 lies out of the horizontal plane by an angle $\varepsilon = H_v/H$. The angle θ defined by the $\vec{J}$ and $\vec{k}$ vectors is $\theta_m - \varepsilon$, where θ_m is the angle between $\vec{k}$ and the horizontal plane, and the net switching angle is $\pi - 2\varepsilon$. The total measured "time-reversal" asymmetry for the ith detector is

$$\begin{aligned} A_t &= \frac{W_i(\theta_+,\phi_i) - W_i(\theta_-,\phi_i)}{W_i(\theta_+,\phi_i) + W_i(\theta_-,\phi_i)} \\ &= \frac{W_i(\theta_m-\varepsilon,\phi_i) - W_i(\pi-\theta_m-\varepsilon,\phi_i)}{W_i(\theta_m-\varepsilon,\phi_i) + W_i(\pi-\theta_m-\varepsilon,\phi_i)} \\ &= A_i + A_v \,, \end{aligned} \tag{C.1}$$

where A_i is the T-odd asymmetry $\propto B_3 P_3^{\,2}(\cos\theta_m) \sin 2\phi_i \sin(\eta+\xi)$

and

$$\begin{aligned} A_v &= \frac{\sum_{k=2,4} Q_k B_k U_k A_k \left[P_k(\cos(\theta_m-\varepsilon)) - P_k(\cos(\pi-\theta_m-\varepsilon))\right]}{2 + \sum_{k=2,4} Q_k B_k U_k A_k \left[P_k(\cos(\theta_m-\varepsilon)) + P_k(\cos(\pi-\theta_m-\varepsilon))\right]} \\ &\simeq \frac{Q_2 B_2 U_2 A_2 (dP_2/d\theta)\, 2\varepsilon}{2 + 2Q_2 B_2 U_2 A_2 P_2(\cos\theta_m)} \\ &= \frac{3Q_2 B_2 U_2 A_2 \sin\theta_m \cos\theta_m\, \varepsilon}{1 + Q_2 B_2 U_2 A_2 P_2(\cos\theta_m)} \,. \end{aligned} \tag{C.2}$$

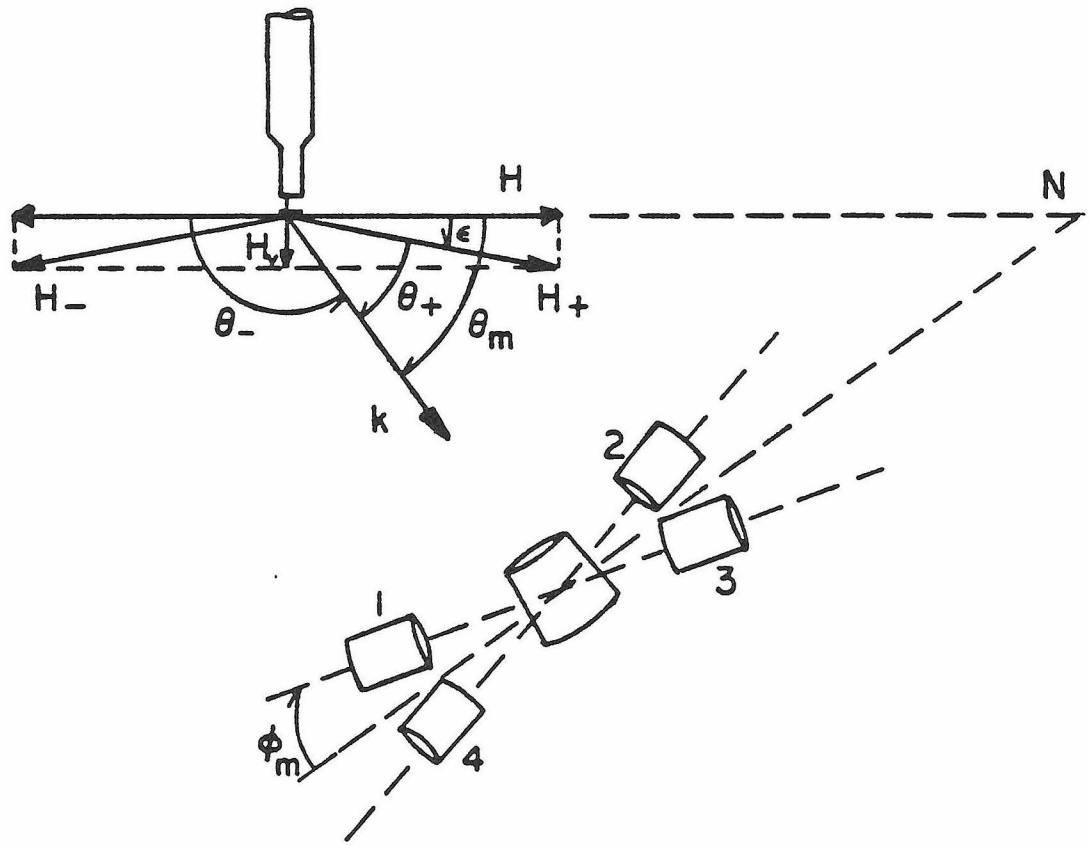

Fig. C.1. Diagram illustrating the effect of a residual vertical field in the source foil.

(The much smaller P_4 term has been neglected.) Thus each detector sees an additional asymmetry proportional to ε. However, the measured asymmetry averaged over all detectors gives

$$A_t = \left[\sum_{i=1}^{4} (A_i + A_v)(-)^{i+1}/\sigma_i^2\right] \Big/ \sum_i (1/\sigma_i^2)$$

$$\simeq 1/4 \sum_{i=1}^{4} \left[(-)^{i+1} A + A_v\right](-)^{i+1}$$

$$= A ,$$

with A the "time-reversal" asymmetry of Eq. (2.8). A vertical-field asymmetry therefore cancels out when averaged over the four polarimeter detectors (assuming the statistical weights σ_i are approximately equal for all detectors).

C.2 The Effect of a Horizontal Field

Let us now consider the effect of a fixed horizontal component of field H_h perpendicular to the switching field, with $\varepsilon = H_h/H$ as shown in Fig. C.2. The previous arguments for a vertical field also hold for the asymmetry A_1 in the intensity distribution seen by the Ge detector (in the horizontal plane of the source), so that

$$A_1 \simeq \frac{3Q_2B_2U_2A_2 \sin\theta \cos\theta \, \varepsilon}{1 + Q_2B_2U_2A_2P_2(\cos\theta)}. \tag{C.3}$$

The fixed horizontal field will additionally result in a net angle

$$\begin{aligned} \phi &\simeq \phi_m - \varepsilon \sin\theta \\ &= \phi_m - \varepsilon' \end{aligned} \tag{C.4}$$

defined by NaI No. 1 and the $\vec{J}$-$\vec{k}$ plane which is no longer $\phi = \phi_m = 45^\circ$. The T-even distribution $W_2(\theta,\phi)$ is hence nonzero, and the imperfectly reversing field will generate an asymmetry A_h seen by the ith detector as follows:

$$\begin{aligned} A_h &= \frac{W_2(\theta,\phi_+) - W_2(\theta,\phi_-)}{2W_1(\theta) + W_2(\theta,\phi_+) + W_2(\theta,\phi_-)} \\ &\simeq \frac{W_2(\theta_m, \phi_i - \varepsilon') - W_2(\theta_m, \phi_i + \varepsilon')}{2W_1(\theta)} \\ &= \left\{ \frac{\sum_{k=2,4} Q_k B_k A_{k2} \, 2\left[\frac{(k-2)!}{(k+2)!}\right]^{1/2} P_k{}^2(\cos\theta_m)}{2 + 2Q_4U_4A_4P_4(\cos\theta_m)} \right\} \left[\cos 2(\phi_i - \varepsilon') - \cos 2(\phi_i + \varepsilon')\right] \end{aligned} \tag{C.5}$$

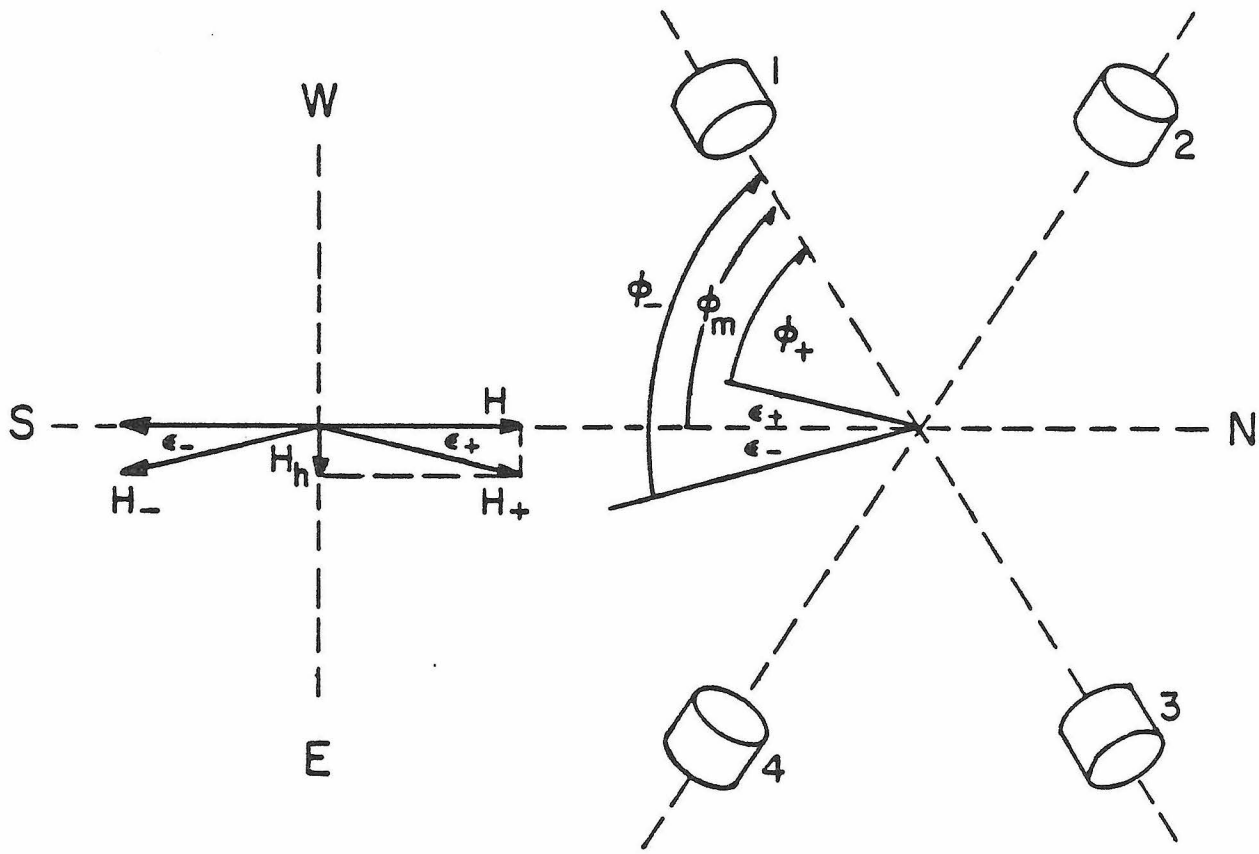

Fig. C.2. Diagram illustrating the effect of a residual field in the plane of the source foil.

$$= (A_p/2)(2 \sin 2\phi_i)\ 2\varepsilon'$$

$$= (-)^{i+1}\ 2\ A_p \sin\theta_m \varepsilon. \qquad (C.6)$$

The expression is braces in (C.5) is precisely the polarization asymmetry A_p of (3.8), divided by 2, and has been so replaced to obtain (C.6). The $(-)^{i+1}$ weighting for each detector is that of the time-reversal asymmetry. The total measured asymmetry will therefore be

$$A_t = A + A_h$$

$$= A + 2\varepsilon \sin\theta_m\ A_p. \qquad (C.7)$$

A_p is negative ($A_p \simeq -0.03$) for the 129 keV line of ^{191}Ir. As illustrated in Fig. C.2 for the polarimeter in the N orientation, an E horizontal field corresponds to a positive $2\varepsilon = \phi_- - \phi_+$; A_h is then negative and the measured asymmetry A_t will be smaller than the (positive) time-reversal asymmetry A. In the S orientation ε is negative and the opposite is true. The A_h contribution cancels out if the two A_t measurements are averaged. A north component of field will similarly result in a negative-contributing asymmetry A_h for the W orientation and an opposite positive contribution for the E orientation. A horizontal field equivalent to that induced by a 4 gauss external field corresponds to $\varepsilon = 2 \times 10^{-3}$ and $|A_h| \simeq 1 \times 10^{-4}$.

REFERENCES

1. J.H. Christenson, J.W. Cronin, V.L. Fitch, and R. Turlay, Phys. Rev. Lett. 13, 138 (1964).
2. R.C. Casella, Phys. Rev. Lett. 21, 1128 (1968); 22, 554 (1969).
3. L. Wolfenstein, Nucl. Phys. B77, 375 (1974).
4. A. Richter, in Symposium on Interaction Studies in Nuclei, Proceedings of the 1975 Mainz Symposium, edited by H. Jachim and B. Ziegler (North-Holland, Amsterdam, 1975).
5. K. Kleinknecht, Annu. Rev. Nucl. Sci. 26, 1 (1976).
6. E.M. Henley, Annu. Rev. Nucl. Sci 19, 367 (1969).
7. I.S. Altarev et al., Pis'ma V Zh. Eksp. & Teor. Fiz. (USSR) 29, 794 (1979).
8. R.J. Blin-Stoyle and F.A. Bezerra Countinho, Nucl. Phys. A211, 157 (1973).
9. W.A. Steyert and K.S. Krane, Phys. Lett. 47B, 294 (1973).
10. K.S. Krane, B.T. Murdoch, and W.A. Steyert, Phys Rev. C 10, 840 (1974).
11. B.T. Murdoch, C.E. Olsen, and W.A. Steyert, Phys Rev C 10, 1475 (1974).
12. S.P. Lloyd, Phys. Rev. 81, 161 (1951).
13. B.A. Jacobsohn and E.M. Henley, Phys. Rev. 113, 234 (1959).
14. F. Boehm, in Hyperfine Structure and Nuclear Radiations, edited by E. Matthias and D.A. Shirley (North-Holland, Amsterdam, 1968), p.279.
15. O.C. Kistner, Phys. Rev. Lett. 19, 872 (1967).
16. M. Atac, B. Chrisman, P. Debrunner, and H. Frauenfelder, Phys. Rev. Lett. 20, 691 (1968).

17. E. Zech, F. Wagner, H.J. Koerner, and P. Kienle in Hyperfine Structure and Nuclear Radiations (see Ref. 14), p 314; E. Zech, Z. Phys. 239, 197 (1970).

18. N.K. Cheung, H.E. Henrikson, E.J. Cohen, A.J. Becker, and F. Boehm, Phys. Rev. Lett. 37, 588 (1976).

19. N.K. Cheung, H.E. Henrikson, and F. Boehm, Phys. Rev. C 16, 2381 (1977).

20. J.L. Gimlett, H.E. Henrikson, N.K. Cheung, and F. Boehm, Phys. Rev. Lett. 42, 354 (1979).

21. J.P. Hannon and G.T. Trammell, Phys. Rev. Lett. 21, 726 (1968).

22. E.M. Henley and B.A. Jacobsohn, Phys. Rev. Lett. 16, 706 (1966).

23. B.R. Davis, S.E. Koonin, and P. Vogel, Phys. Rev. A (to be published).

24. G.T. Trammell and J.P. Hannon, Phys. Rev. 180 337 (1969); J.P. Hannon and G.T. Trammell, Phys. Rev. 186, 306 (1969).

25. Yu. M. Kagan, A.M. Afanas'ev, and V.K. Voitovetskii, Pis'ma V Zh. Eksp. & Teor. Fiz. (USSR) 9, 155 (1969) [JETP Lett. 9, 91 (1969)].

26. H.C. Goldwire, Jr. and J.P. Hannon, Phys. Rev. B 16, 1875 (1977).

27. R.M. Steffen, Los Alamos Scientific Laboratory Report No. LA-4565-MS, 1971 (unpublished).

28. R.M. Steffen and K. Alder, in The Electromagnetic Interaction in Nuclear Spectroscopy, edited by W.D. Hamilton (North-Holland, Amsterdam, 1975), p.505.

29. K.S. Krane, Los Alamos Scientific Laboratory Report No. LA-4677, 1971 (unpublished).

30. K.S. Krane, Nucl. Data Tables 11, 407 (1973).

31. D. Salomon and D.A. Shirley, Phys. Rev. B 9, 29 (1974).

32. G. Eska, E. Hagn, T. Butz, and P. Kienle, Phys. Lett. 36B, 328 (1971), report a value $\mu = 6.03\ \mu_n$ for an NMR measurement sensitive to the product of μ and H_{hf}, taking $H_{hf} = 1.405$ MG. Assuming the more recent value $H_{hf} = 1.481$ MG of Ref. 31, μ becomes $\mu = 5.72$.

33. K.S. Krane, At. Data Nucl. Data Tables 18, 137 (1976); K.S. Krane and W.A. Steyert, Phys. Rev. C 7, 1555 (1973).

34. A.J. Becker, H.E. Henrikson, and D.C. Cook, Nucl. Instrum. 108, 291 (1973).

35. N.K. Cheung, Ph.D. thesis, Appendix, 1976, California Institure of Technology (unpublished).

36. K.S. Krane, Nucl. Instrum. 98, 205 (1972).

37. K.S. Krane and W.A. Steyert, Phys. Rev. C 9, 2063 (1974).

38. E. Matthias and R.J. Holliday, Phys. Rev. Lett. 17, 897 (1966).

39. E.J. Cohen, A.J. Becker, N.K. Cheung, and H.E. Henrikson, Hyperfine Int. 1, 193 (1975).

40. K.D. Baker and W.D. Hamilton, Nucl. Instrum. 86, 77 (1970).

41. E. Lipworth, H.L. Garvin, and T.M. Green, Phys. Rev. 119, 2022 (1960).

42. P.K. James, N.J. Stone, and H.R. Foster, Phys Lett. 48A, 237 (1974).

43. B.K.S. Koene and H. Postma, Nucl. Phys. A219, 563 (1974).

44. ICN Isotope and Nuclear Division, 2727 Campus Dr., Irvine, California 92664.

45. P.G.E. Reid, M. Sott, N.J. Stone, D. Spanjaard, and H. Bernas, Phys. Lett. 25A, 396 (1967).

46. H. deWaard, R. J. Cohen, S.R. Reintsema, and S.A. Drentje, Phys. Rev. B 10, 3760 (1974).

47. D. Visser, L. Niesen, H. Postma, and H. deWaard, Phys. Rev. Lett. 41, 882 (1978).

48. G.W. Wang, A.J. Becker, L.M. Chirovsky, J.L. Groves, and C.S. Wu, Phys. Rev. C 18, 476 (1978).

49. S.H.E. Corporation, 4174 Sorrento Valley Blvd., San Diego, California, 92121.